The Astrophysical Journal, 800:12 (17pp), 2015 February 10 doi:10.1088/0004-637X/800/1/12

THE MOST METAL-POOR DAMPED Lyα SYSTEMS: AN INSIGHT INTO DWARF GALAXIES AT HIGH-REDSHIFT*

Ryan J. Cooke[1,4], Max Pettini[2], and Regina A. Jorgenson[3]
[1] Department of Astronomy and Astrophysics, University of California Santa Cruz, Santa Cruz, CA 95064, USA; rcooke@ucolick.org
[2] Institute of Astronomy, Madingley Road, Cambridge, CB3 0HA, UK
[3] Institute for Astronomy, University of Hawaii, 2680 Woodlawn Drive, Honolulu, HI 96822, USA
Received 2014 June 26; accepted 2014 December 1; published 2015 February 4

ABSTRACT

In this paper we analyze the kinematics, chemistry, and physical properties of a sample of the most metal-poor damped Lyα systems (DLAs), to uncover their links to modern-day galaxies. We present evidence that the DLA population as a whole exhibits a "knee" in the relative abundances of the α-capture and Fe-peak elements when the metallicity is [Fe/H] $\simeq -2.0$, assuming that Zn traces the buildup of Fe-peak elements. In this respect, the chemical evolution of DLAs is clearly different from that experienced by Milky Way halo stars, but resembles that of dwarf spheroidal galaxies in the Local Group. We also find a close correspondence between the kinematics of Local Group dwarf galaxies and of high-redshift metal-poor DLAs, which further strengthens this connection. On the basis of such similarities, we propose that the most metal-poor DLAs provide us with a unique opportunity to directly study the dwarf galaxy population more than ten billion years in the past, at a time when many dwarf galaxies were forming the bulk of their stars. To this end, we have measured some of the key physical properties of the DLA gas, including their neutral gas mass, size, kinetic temperature, density, and turbulence. We find that metal-poor DLAs contain a warm neutral medium with $T_{\rm gas} \simeq 9600$ K predominantly held up by thermal pressure. Furthermore, all of the DLAs in our sample exhibit a subsonic turbulent Mach number, implying that the gas distribution is largely smooth. These results are among the first empirical descriptions of the environments where the first few generations of stars may have formed in the universe.

Key words: galaxies: abundances – galaxies: dwarf – galaxies: evolution – Local Group – quasars: absorption lines

1. INTRODUCTION: LOW-METALLICITY GALAXIES

The population of dwarf galaxies represents the least luminous, least massive, and perhaps the most numerous galaxies at all redshifts in the observed universe. However, despite their great number, just a handful of these galaxies have been firmly identified, owing to their intrinsically low luminosities (see McConnachie 2012 for a continuously updated list of systems). Typically, these galaxies are very metal-poor and are highly varied in their physical properties (Mateo 1998; Tolstoy et al. 2009). At present, our understanding of the chemical evolution and buildup of stellar mass in these galaxies involves a careful "archaeological"study of their present-day physical and chemical properties.

1.1. The Nearby Universe

For many decades, it has been appreciated that a color–magnitude diagram (CMD) encodes the evolutionary sequence of stellar populations. Variations in a population's age, metallicity, star formation rate, and stellar initial mass function (IMF) can in principle be recovered through a synthetic CMD analysis (e.g., Tolstoy & Saha 1996). This has proven to be a highly successful approach to studying the star formation history (SFH) of Local Group dwarf galaxies (see the review by Tolstoy et al. 2009, and references therein). For example, from the analysis of their CMDs, Weisz et al. (2014a) found that dwarf spheroidal (dSph) galaxies in the vicinity of the Milky Way (MW) experienced highly varied levels of star formation more than 1 Gyr ago, and show little to no evidence for recent star formation activity. Beyond the MW, CMD analyses for a large sample of nearby dwarf galaxies with a range of morphological types have further highlighted the great diversity in SFHs of low-mass galaxies (Weisz et al. 2011). In these systems, a considerable fraction of their stellar mass was in place by redshift $z \sim 1$, regardless of their present-day morphological type. Furthermore, these systems appear to have experienced significant levels of ancient star formation that took place at least 10 Gyr ago, at redshifts $z \gtrsim 2$. Such studies have emphasized that the high-redshift universe potentially offers a rich perspective on the evolution of low-mass galaxies.

An alternative and complementary approach to studying the evolution of dwarf galaxies involves detailed chemical abundance measurements of individual member stars (Shetrone et al. 1998; Bonifacio et al. 2000; Shetrone et al. 2001). These stars condensed from gas that was enriched by the cumulative products of previous stellar generations. The overall metallicity distribution function therefore contains precious information on the chemical evolution and SFH of dwarf galaxies. A timescale for the chemical enrichment can then be teased out from the *relative* metal abundances; stars of different mass and metallicity synthesize elements in different proportions and release their nucleosynthetic products into the surrounding interstellar medium (ISM) at different times. Therefore, deciphering the chemistry of a dwarf galaxy provides key information on the timescales and dominant sources of enrichment. For example, stars in the mass range $10 \lesssim m_\star \lesssim 100\,M_\odot$ end their life as Type II

* Based on observations collected at the European Organisation for Astronomical Research in the Southern Hemisphere, Chile (VLT program IDs: 60.A-9022(A), 65.O-0063(B), 65.O-0296(A), 67.A-0022(A), 67.A-0078(A), 68.A-0600(A), 68.B-0115(A), 70.A-0425(C), 078.A-0185(A), 080.A-0014(A), 082.A-0544(A), 083.A-0042(A), 083.A-0454(A), 085.A-0109(A), 086.A-0204(A)), and at the W. M. Keck Observatory which is operated as a scientific partnership among the California Institute of Technology, the University of California and the National Aeronautics and Space Administration. The Observatory was made possible by the generous financial support of the W. M. Keck Foundation. Keck telescope time was partially granted by NOAO, through the Telescope System Instrumentation Program (TSIP). TSIP is funded by NSF.
[4] Hubble/Morrison Fellow.

supernovae (SNe) on relatively short timescales (<30 Myr), and are the primary source of the α-capture elements, in addition to some Fe-peak elements. On the other hand, Type Ia SNe, which operate on much longer timescales (∼1 Gyr),[5] predominantly yield Fe-peak elements. Thus, one initially expects a plateau in the ratio of α/Fe-peak elements (due to Type II SNe) until Type Ia SNe explode and contribute their Fe-peak elements, thereby lowering the α/Fe ratio. The downturn in the α/Fe ratio (a.k.a. the "knee") therefore tracks the SFH of the galaxy and its ability to retain metals (see, e.g., the discussion by Tinsley 1979; Wheeler et al. 1989).

Of the known dwarf galaxies in the local universe, only those in orbit around the MW have resolved, bright stellar populations that allow one to measure the metallicities of individual member stars using high resolution spectrographs, and thereby study their chemical evolution in fine detail. In the last decade, there have been many efforts to trace the chemical history of the brightest MW dSph galaxies (Bonifacio et al. 2004; Monaco et al. 2005; Sbordone et al. 2007; Koch et al. 2008; Cohen & Huang 2009, 2010; Letarte et al. 2010; Hendricks et al. 2014). For typical MW dSphs, the knee in the α/Fe ratio occurs at roughly 1/100 of solar metallicity (i.e., [Fe/H] ~ -2.0),[6] signaling that Type Ia SNe contributed their enrichment at an early stage of the dwarf galaxy's chemical evolution. This observation is very much in agreement with inferences on the SFH of the MW dSphs from CMD analyses—the luminous MW dSph galaxies experienced modest levels of "bursty" star formation over an extended period.

Deep and wide-area surveys for these low-luminosity dSph galaxies, made possible by the Sloan Digital Sky Survey (SDSS; York et al. 2000), have uncovered a faint galaxy population—termed the ultra-faint dwarf (UFD) galaxies—that extend the known suite of galaxies to even fainter luminosities (Willman et al. 2005a, 2005b; an up-to-date list can be found in Belokurov 2013). These "ultra-faint"galaxies appear to be an extension of the "classical" dSph galaxy population to much lower luminosities (Belokurov 2013; Walker et al. 2013). Detailed CMD analyses of the UFDs suggest that these galaxies assembled a significant fraction of their present-day stellar mass prior to redshift $z \sim 2$ (Weisz et al. 2014a). Intriguingly, there is also evidence for a small number of carbon-enhanced metal-poor stars showing normal (or very low) abundances of the neutron-capture elements (i.e., the so-called CEMP-no stars) associated with both the Segue 1 and Boötes I UFDs (Norris et al. 2010; Lai et al. 2011; Gilmore et al. 2013; Frebel et al. 2014). It is thought that such stars may have condensed out of gas that was solely enriched by the first stars (Ryan et al. 2005; Cooke & Madau 2014), making the UFD galaxies the modern-day, surviving relics of the minihalos that hosted the very first generation of stars (e.g., Frebel & Bromm 2012).

1.2. The High-redshift Universe

Given the importance of dwarf galaxies in the early buildup of cosmic structure, as well as the possibility to probe the chemistry of the first stars and the formation of the second stellar generation, it is of great interest to study the dwarf galaxy population at high-redshift when they were in the process of building their stellar mass. However, this is a very difficult prospect in practice. For example, the current stellar population in Boötes I (at a distance of ∼60 kpc; Belokurov et al. 2006) would correspond to a rest-frame visual magnitude of $m_V \simeq 41$ at redshift $z \sim 3$, more than 10,000 times fainter than the faintest objects detected in the *Hubble Space Telescope (HST)* extreme deep field (Illingworth et al. 2013). Some assistance can be provided by gravitational lensing (Amorín et al. 2014; Alavi et al. 2014), and indeed this is one of the primary goals of the *HST Frontier Fields*. However, such observations are unlikely to reach the lowest luminosity dwarfs and will in any case be restricted to the relatively small volumes magnified by the gravitational lenses. Other "direct detection" studies have instead searched for the putative Lyα emission arising from galaxies that are experiencing very low levels of star formation (Rauch et al. 2008) or via fluorescent Lyα emission of gas-rich galaxies that are presumably on the verge of star formation (Cantalupo et al. 2012). While these efforts undoubtedly contribute to our view of high-redshift, low-mass galaxies, they are unable to simultaneously provide detailed physical and chemical insights into star formation in the low-metallicity regime.

The work by Weisz et al. (2011, 2014a) has indicated that many dwarf galaxies formed a considerable fraction of their present-day stellar population between redshifts $z = 1$ and 4. Therefore, at some point in their evolution, the local dwarf galaxies must have contained a reservoir of cold, neutral gas that allowed them to form their small pool of stars. Such conditions are satisfied by the generic properties of damped Lyman α systems (DLAs), absorption systems that are easily identified by their strong H I Lyα absorption feature along the line of sight to an unrelated, background light source (typically a quasar). By definition, DLAs have column densities of neutral hydrogen in excess of $N(\mathrm{H\,I}) \geqslant 10^{20.3}$ H I atoms cm^{-2} (Wolfe et al. 1986; for a review, see Wolfe et al. 2005) and are typically enriched to 1/30 of the solar metallicity at redshift $z \sim 3$ (Pettini et al. 1997; Prochaska et al. 2003; Rafelski et al. 2012; Jorgenson et al. 2013). This typical metallicity is also known to evolve modestly with redshift (Rafelski et al. 2012; Jorgenson et al. 2013); an extrapolation of this relation to the present day would imply that DLAs at redshift $z \sim 0$ should be enriched to ∼1/10 of the solar metallicity, similar to the metallicity of the Fornax dSph (e.g., Kirby et al. 2011b). Furthermore, any reasonable extrapolation of the stellar mass–metallicity relation of DLAs proposed by Christensen et al. (2014) would suggest that a typical DLA has a stellar mass consistent with a dwarf galaxy (∼10^{8-9} $M_\odot$; see also, Møller et al. 2013).

Since the inception of DLA research, there has been a considerable effort to image the host galaxies of DLAs or catch them in line emission. Despite the efforts of many, the typical DLA population has largely evaded detection. In all cases, the imaged DLAs are either: (1) biased toward the higher end of the DLA metallicity distribution function and are, consequently, those most actively forming stars; (2) undetected along the quasar sightline, but a proximate ∼$L^\star$ galaxy is seen at large impact parameters; or (3) completely undetected. Despite the difficulty of recognizing a DLA host galaxy against the glare of the backdrop quasar, there are a handful of solid detections at $z \gtrsim 2$ (Lowenthal et al. 1995; Bunker et al. 1999; Kulkarni et al. 2000; Christensen et al. 2009; Fynbo et al. 2010; Krogager et al. 2012, 2013; Noterdaeme et al. 2012; Péroux et al. 2012; Jorgenson

[5] We note, however, that the delay time distribution for Type Ia SNe may have a contribution from prompt Type Ia SNe (Mannucci et al. 2006), which operate on shorter timescales.

[6] Throughout this paper, we adopt the standard notation [X/Y] ≡ log N(X)/N(Y) − log (X/Y)$_\odot$, where N(X)/N(Y) is the number abundance ratio of element X relative to element Y, and the ⊙ symbol refers to the solar value, taken from Asplund et al. (2009).

& Wolfe 2014; Fumagalli et al. 2014) that suggest that DLAs are a "mixed bag."

Clues to the nature of DLAs from cosmological hydrodynamic simulations have shown that the DLA cross-section primarily comes from galaxies in halos of mass 10^9–10^{11} $M_\odot$ at $z \sim 3$ (Pontzen et al. 2008; Tescari et al. 2009; Fumagalli et al. 2011; Cen 2012; van de Voort et al. 2012; Bird et al. 2013; Rahmati & Schaye 2014). Therefore, the lack of nearby $L^\star$ galaxies in the proximity of DLAs, the peak of the DLA halo distribution ($\sim 10^{10}$ $M_\odot$), the peak of the DLA metallicity distribution at redshift $z \simeq 3$ (1/30 solar), and the extrapolation of the DLA redshift–metallicity relation to redshift $z = 0$, all point to a *typical* DLA being associated with a dwarf galaxy. However, the measured bias factor of DLAs (Cooke et al. 2006; Font-Ribera et al. 2012; Barnes & Haehnelt 2014), under some model assumptions, places DLAs in a typical host halo of mass $10^{10.5}$–10^{12} $M_\odot$ at redshift 2–3.

Several studies over the past few years have begun to focus on the metal-poor tail of the DLA metallicity distribution function (Pettini et al. 2008; Penprase et al. 2010; Cooke et al. 2011a, 2011b, 2012; Dutta et al. 2014), which currently extends down to [Fe/H] = −3.45 ($z_{\rm abs} = 3.6966$ toward J0140−0829; Ellison et al. 2010; Cooke et al. 2011b). Most of the gas in these near-pristine systems has not yet been processed through generations of stars, and has therefore retained a primordial composition of the light elements (Pettini & Cooke 2012; Cooke et al. 2014). Indeed, some of the most metal-poor DLAs may have only seen the enrichment from a single generation of Population III stars (e.g., Cooke et al. 2011a; herein, we update the chemical composition of this DLA; see Appendix B). More generally, the most metal-poor DLAs (with metallicities [Fe/H] $\lesssim -2.0$) exhibit an enhancement in their α/Fe ratio, consistent with that seen in Local Group dwarf galaxies and metal-poor Galactic halo stars (Cooke et al. 2011b; Rafelski et al. 2012).

The most metal-poor DLAs at high-redshift can evidently play an important role in furthering our understanding of the formation of stars in extremely low-metallicity environments and at early times. Moreover, such systems provide the only avenue in the foreseeable future to *directly* probe the early evolution of the smallest galaxies. In this paper, we present measurements of the most basic physical properties of the metal-poor DLA population (e.g., their kinetic temperature and volume density). We also provide the first crucial links between high-redshift metal-poor DLAs and near-field dwarf galaxies.

In the following section we discuss the high-redshift DLA sample used throughout this paper. To better understand the nature of these systems, we compare the kinematics and chemistry of the metal-poor DLA population with those of Local Group galaxies in Sections 3 and 4, respectively. The physical properties of a smaller sample of low-metallicity DLAs (those with the best data for the purpose) are derived in Section 5, giving new insights into the physical state of the neutral gas in these systems. In Section 6, we discuss the nature and evolution of the most metal-poor DLAs, before summarizing the main findings of this work in Section 7.

2. THE SAMPLE OF METAL-POOR DLAs

The high-redshift DLA sample considered here consists of the systems published in our recent surveys (Pettini et al. 2008; Cooke et al. 2011b, 2013, 2014) which focus on DLAs with iron abundance [Fe/H] $\leqslant -2.0$. We omit two systems considered in those works (toward the QSOs J0311−1722 and J1016+4040) where we were unable to measure [Fe/H], but we add one new system (in the spectrum of J1111+1332), and reanalyze another (in J0035−0918; Cooke et al. 2011a). For further details on these two systems, see Appendix B. The data that are presented in this paper were all acquired with high-resolution echelle spectrographs ($R \gtrsim 30{,}000$), including the W. M. Keck Observatory's High Resolution Echelle Spectrograph (HIRES) and the Very Large Telescope's Ultraviolet and Visual Echelle Spectrograph (UVES). Relevant properties of the DLA sample considered here are collected in Table 1. In Section 5, we refine our sample selection to consider only the DLAs where the contributions of thermal and turbulent broadening to the absorption line profiles could be measured separately with sufficient precision (in many cases turbulent broadening dominates over thermal broadening, so that the latter cannot be determined independently). For further details, see Appendix A.

3. THE KINEMATICS OF METAL-POOR DLAs

The kinematic information extracted from the analysis of metal absorption lines in DLAs is one of the key observables that has been used to infer the nature of the DLA host galaxy population. The first detailed investigation of DLA kinematics was presented by Prochaska & Wolfe (1997). These authors introduced a test statistic, known as v_{90}, which measures the velocity interval covering the innermost 90% of the total optical depth of unsaturated metal absorption. In general, DLAs exhibit a broad range in their v_{90} statistic; the distribution of values peaks near 70 km s^{-1} with a high-velocity tail that extends out to $\sim$450 km s^{-1}. Using a suite of Monte Carlo simulations, Prochaska & Wolfe (1997) explored a variety of simple galaxy models to conclude that the kinematics of the DLA population are mostly consistent with thick, rapidly rotating disks. An alternative possibility was proposed shortly after by Haehnelt et al. (1998) using cosmological *N*-body hydrodynamic simulations. These authors showed that the distribution of asymmetries and velocity widths of DLA metal absorption lines can be naturally explained in the context of hierarchical galaxy formation, where the kinematics of DLAs arise from the combination of ordered and random motions, in addition to infall and merging (see, however, Prochaska & Wolfe 2010). Since these early works, cosmological hydrodynamic simulations have advanced substantially, and yet they still have difficulty in reproducing the large velocity widths exhibited by some DLAs (Pontzen et al. 2008; Tescari et al. 2009; Cen 2012). A potential resolution to this problem has recently been proposed by Bird et al. (2014), who interpret the largest velocity widths as arising from the chance alignment of a DLA host galaxy and a metal-enriched Lyman limit system residing in a filament near the DLA (see, e.g., Pettini et al. 1983).

By combining the measured velocity widths and metallicities of damped Lyα systems, several authors have proposed that DLAs obey a "mass–metallicity" relation (Ledoux et al. 2006; Murphy et al. 2007; Prochaska et al. 2008; Jorgenson et al. 2013; Neeleman et al. 2013). Using the v_{90} velocity width as a proxy for the mass of the DLA host galaxy, DLAs with the largest velocity widths statistically show the highest metallicities. Thus, it appears that the gas distribution broadly traces the gravitational potential of the host galaxy. In this picture, DLAs that exhibit the lowest metallicities should also exhibit the most quiescent kinematics, and thus be related to the lowest mass galaxies.

Thus, it is of interest to compare the kinematics of the most metal-poor DLAs to those of Local Group dwarf galaxies. The latter are typically characterized by the 1σ line-of-sight

Table 1
The Kinematics and Chemistry of Metal-poor DLAs

QSO Name	z_{abs}	v_{68} (km s^{-1})	[Fe/H][a]	[Si/Fe][a]
Q0000−2620	3.390	12.0	-2.01 ± 0.09	$+0.15 \pm 0.04$
J0035−0918	2.340	1.6	-2.94 ± 0.06	$+0.37 \pm 0.07$
HS 0105+1619	2.537	4.2	-2.10 ± 0.05	$+0.25 \pm 0.06$
Q0112−306	2.418	19.4	-2.64 ± 0.09	$+0.25 \pm 0.06$
J0140−0839	3.697	47.5	-3.45 ± 0.24	$+0.70 \pm 0.21$
J0307−4945	4.467	141	-1.93 ± 0.20	$+0.43 \pm 0.18$
J0831+3358	2.304	18.5	-2.39 ± 0.16	$+0.38 \pm 0.08$
Q0913+072	2.618	14.6	-2.77 ± 0.05	$+0.27 \pm 0.02$
J1001+0343	3.078	6.5	-3.48 ± 0.27	$+0.62 \pm 0.27$
J1037+0139	2.705	9.8	-2.44 ± 0.08	$+0.40 \pm 0.04$
Q1108−077	3.608	17.4	-1.96 ± 0.07	$+0.42 \pm 0.03$
J1111+1332	2.271	3.0	-2.27 ± 0.04	$+0.32 \pm 0.02$
J1337+3152	3.168	18.5	-2.74 ± 0.30	$+0.06 \pm 0.26$
J1340+1106	2.508	24.6	-2.04 ± 0.06	$+0.18 \pm 0.03$
J1340+1106	2.796	10.4	-2.15 ± 0.06	$+0.32 \pm 0.03$
J1358+6522	3.067	3.4	-2.60 ± 0.07	$+0.31 \pm 0.03$
J1419+0829	3.050	17.3	-2.27 ± 0.11	$+0.24 \pm 0.02$
J1558−0031	2.702	12.4	-2.03 ± 0.04	$+0.26 \pm 0.05$
J1558+4053	2.554	8.2	-2.70 ± 0.07	$+0.21 \pm 0.07$
Q1946+7658	2.844	7.0	-2.50 ± 0.06	$+0.32 \pm 0.02$
Q2059−360	3.083	32.7	-1.97 ± 0.08	$+0.34 \pm 0.06$
J2155+1358	4.212	26.4	-2.15 ± 0.25	$+0.28 \pm 0.23$
Q2206−199	2.076	7.5	-2.55 ± 0.04	$+0.30 \pm 0.02$

Note. [a] We have adopted solar abundances of $12 + \log(\mathrm{Si/H})_\odot = 7.51$ and $12 + \log(\mathrm{Fe/H})_\odot = 7.47$ from Asplund et al. (2009).

dispersion of projected stellar motions or, if the galaxy still bears gas, from the H I 21 cm line emission profile. In both cases, the galaxy's kinematics are quantified by considering the 68 per cent interval of the tracer kinematics.

Therefore, to facilitate a comparison between $z \sim 3$ DLAs and Local Group galaxies, we define a new velocity width statistic for DLAs, hereafter denoted v_{68}, which is qualitatively similar to the v_{90} statistic proposed by Prochaska & Wolfe (1997). Specifically, v_{68} is the velocity interval containing the innermost 68% of the total optical depth. Although our v_{68} statistic cannot be directly related to a *stellar* velocity dispersion, as measured in the Local Group dwarf galaxies, it provides a simple conversion to the velocity dispersion of the gas. Furthermore, compared with the v_{90} statistic, v_{68} is much less sensitive to weak absorption that is well separated from the dominant optical depth. In order to measure v_{68} from the observed profiles of the absorption lines in a DLA, it is necessary to correct for two sources of broadening that are unrelated to the bulk motions of the gas, namely thermal (i.e., microscopic) and instrumental (i.e., due to the spectrograph with which the data were recorded) broadening. In the most quiescent DLAs, where the absorption is confined to a single velocity component, the correction is straightforward (if the thermal and instrumental broadening are known). In this case, $v_{68} \equiv 2\sigma_{\rm los} = \sqrt{2}\, b_{\rm turb}$.

While it is generally the case that the velocity structure of DLAs with [Fe/H] $\leqslant -2.0$ is relatively simple, in many of the DLAs in Table 1 the absorption is spread over a few velocity components. In such cases, we employed the following procedure to determine v_{68}. First, we generated synthetic Si II (or Fe II) line profiles for each system using only the column densities and turbulent broadening derived from the cloud model that best fits the absorption lines as described in Appendix A (i.e., we did not include thermal and instrumental broadening for the synthetic profiles). Si II and Fe II are the optimum species to use for measuring the velocity fields in these DLAs, since there are generally many Si II and Fe II lines of widely different oscillator strengths, allowing the optical depth to be determined for the full range of velocities over which absorption takes place. Furthermore, of the lines that are often seen in metal-poor DLAs, Si II and Fe II are the least affected by thermal broadening.[7] We then converted the synthetic line profiles to an optical depth profile, and calculated the velocity interval containing the innermost 68 per cent of the total integrated optical depth. Finally, we relate our velocity statistic to the 1σ line-of-sight velocity dispersion by the relation $\sigma_{\rm los} = v_{68}/2$. We note that our analysis only considers the velocity width traced by the low ion metal absorption lines (i.e., C^+, O^0, Si^+, Fe^+), which are known to predominantly trace the H I gas.

The full sample of DLAs for which we have measured v_{68} is collected in Table 1, which also includes values of [Fe/H] "metallicity" and of [Si/Fe], representative of the ratio of α-capture to Fe-peak elements. The data in the last two columns were culled from the references given in Section 2. In Figure 1, we compare the measured kinematics of the DLAs in our sample to those of Local Group galaxies as compiled by McConnachie (2012). To allow for a closer comparison to the MW dSph population, we also present a zoom-in version of this comparison in Figure 2, where we have placed a red circle around the galaxies that have been discovered since the start of the SDSS survey (i.e., those classified as UFDs). There is evidently a very close correspondence between the kinematics and metallicity for the galaxies displayed in Figures 1 and 2 despite the diversity of techniques employed to measure these two quantities.

For a given DLA, we are unable to make a direct connection between our v_{68} statistic and the DLA host potential; since we are unaware of the geometry of the DLA host galaxy, this connection may depend on the inclination of the DLA relative to the sightline probed by the quasar. However, for a sample of systems *at a given metallicity*, each DLA will be intersected at a random inclination angle, so that statistically we may be justified in considering the range of velocity widths exhibited by DLAs at a given metallicity. From inspection of Figures 1 and 2, it can be seen that systems with higher velocity widths tend to have higher metallicities. Similarly, the lowest velocity width systems are associated with the lowest metallicity DLAs. We therefore conclude that the most metal-poor DLAs are generally associated with the lowest mass galaxies that can potentially still form stars at $z \sim 3$.

A clear outlier in the velocity width–metallicity relation for metal-poor DLAs is the DLA toward J0140−0839 (Ellison et al. 2010; included in Table 1 but not shown in Figures 1 and 2 as it is off-scale in those plots). This DLA has one of the highest velocity width measurements of our sample and one of the lowest metallicities. This example highlights the main caveat of our technique; with quasar absorption line spectroscopy, we are unable to distinguish between a DLA in a single halo with a broad velocity distribution or two individual DLAs in close proximity with a small relative velocity along the line of sight. Given that this system exhibits two distinct absorption components, separated by $\sim$45 km s^{-1}, each with $v_{68} \simeq$ 6–10 km s^{-1}, we speculate that its abnormally high velocity width may result from a chance alignment or interaction

[7] For systems where v_{68} was at least twice the instrumental FWHM, we found that v_{68} can accurately be measured directly from the data, without the need to generate synthetic profiles that ignore the thermal and instrumental contributions to the line broadening.

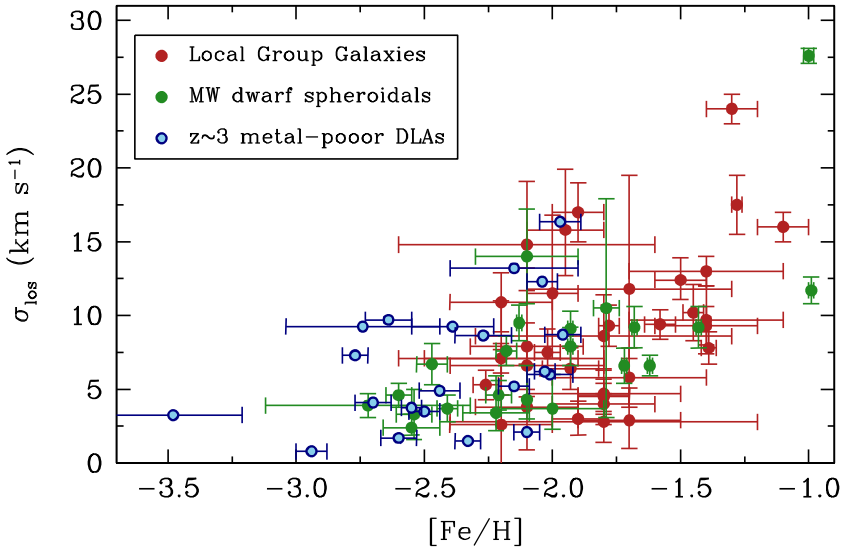

Figure 1. Line-of-sight stellar velocity dispersions and metallicities for a sample of nearby low-metallicity galaxies (red and green symbols; McConnachie 2012) are compared to the most metal-poor DLAs at $z \simeq 3$ (blue symbols). The green symbols highlight the Milky Way dwarf spheroidal galaxies.

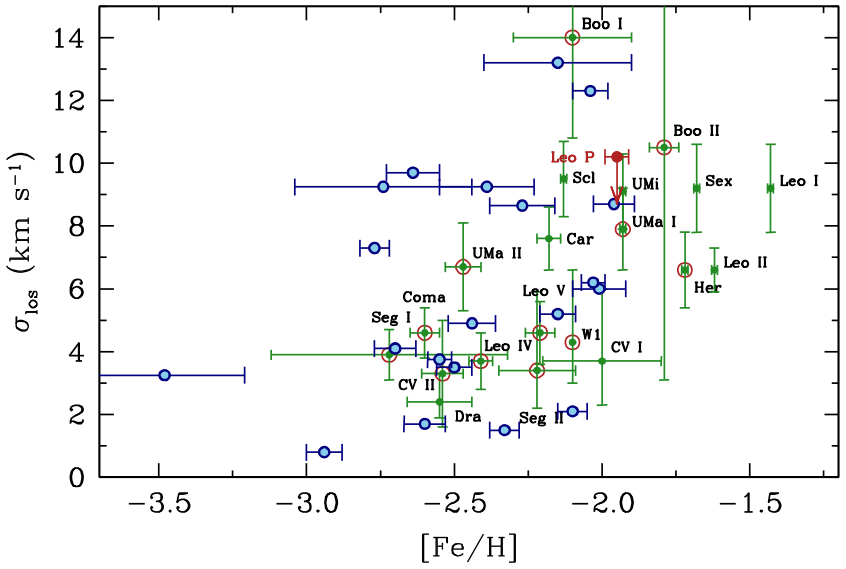

Figure 2. Zoomed in version of Figure 1, comparing only the Milky Way dwarf spheroidals (green symbols; labeled) and the most metal-poor DLAs (blue symbols). The green symbols with red circles correspond to the ultra-faint dwarf galaxies, with total luminosities $\leqslant 10^5\ L_\odot$. We also show the recently discovered nearby gas-rich dwarf galaxy Leo P, where the velocity dispersion is measured from H I 21 cm observations and the Fe abundance is derived from the associated H II region, assuming [Fe/H] = [O/H] −0.4 (red dot; Giovanelli et al. 2013; Skillman et al. 2013). We consider the line-of-sight velocity dispersion for Leo P as an upper limit, since thermal broadening of the line profile may contribute to the line width.

of two very metal-poor DLAs (which, coincidentally, are also close to the QSO redshift).

Clearly, a *direct* comparison between the kinematics of redshift $z \sim 3$ metal-poor DLAs and Local Group dwarf galaxies is fraught with uncertainty, given the different physics that operates on gas versus stars. Nevertheless, on the basis of this comparison, we conclude that the general trend and range of velocity widths exhibited by the most metal-poor DLAs are similar to those seen in nearby dwarf galaxies.

4. THE CHEMISTRY OF METAL-POOR DLAs

The chemical composition and relative element abundances of DLAs provide crucial information on the chemical evolution, SFH, and ultimately the nature of the host galaxies that give rise to the absorption. In this section, we present the current complement of data that allows us to infer the most likely SFH of typical DLAs, as traced by the relative abundance of α-capture and Fe-peak elements. At metallicities less than $\sim$1/100 of solar, the production of α elements in DLAs is best traced by considering the Si II ion, which has numerous transitions with a variety of oscillator strengths and over a range of wavelengths that are redshifted into a convenient portion of the visible spectrum at redshifts $z = 2$–3. For the same reasons, the most reliable tracer of the Fe-peak elements at such metallicities is Fe II.

For DLAs with metallicities greater than $\sim$1/100 of solar, some α-capture and Fe-peak elements may suffer from depletion onto dust grains (Pettini et al. 1997; Akerman et al. 2005; Vladilo et al. 2011) so that the [Si/Fe] abundance measured in the gas phase may be different from the intrinsic [α/Fe] abundance set by chemical evolution. To avoid the effects of dust depletion, S and Zn are often considered the most appropriate combination to trace the relative abundance of α/Fe in the ISM; both S and

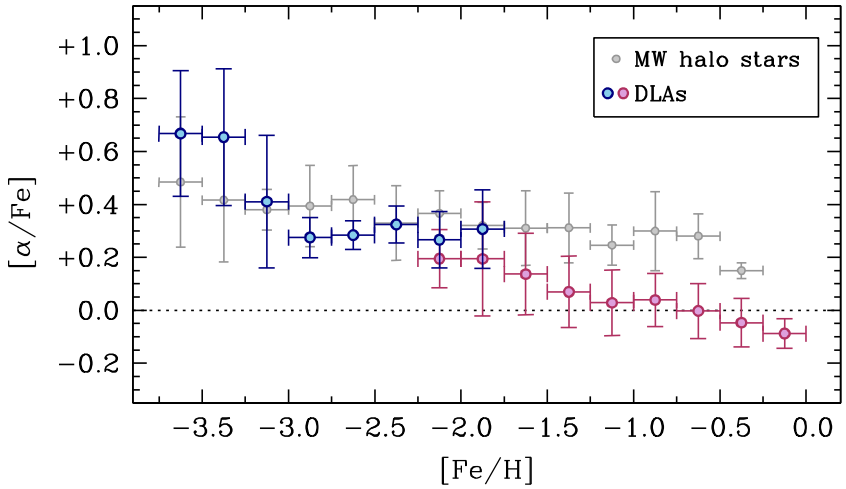

Figure 3. [α/Fe] ratio in DLAs (red symbols denote [S/Zn] and [Zn/H] from Vladilo et al. 2011; blue symbols are for [Si/Fe] and [Fe/H] from our work) are compared to the typical [α/Fe] measured in Milky Way halo stars (gray symbols; Venn et al. 2004). For every 0.25 dex metallicity bin, we plot the mean value of the population, weighted by the errors, and represent the 1σ dispersion in the population with error bars. The horizontal dotted line is drawn at the solar value of the α/Fe ratio. Note that the evolution of [α/Fe] for DLAs would be slightly different if [Zn/Fe] $\neq$ 0.0 when [Fe/H] > -2.0 (see text for the relevant discussion).

Zn have very little affinity for dust grains and, in any case, have an almost identical condensation temperature. Moreover, both S II and Zn II offer multiple transitions that are usually straightforward to measure and rarely suffer from saturation.[8]

However, with current telescope facilities, the strongest Zn II absorption lines become too weak to be reliably measured when the DLA metallicity is $\lesssim$1/100 of solar. Therefore, in order to track the full behavior of the α/Fe ratio in DLAs, we must combine measurements of [Si/Fe] at low-metallicity with [S/Zn] measures at high metallicity. While using different element ratios in different metallicity regimes is clearly not ideal, we believe that systematic offsets between these two pairs of elements are likely to be small. Combining measurements of Si and S seems justified, since detailed nucleosynthesis calculations of massive stars have illustrated that Si and S are produced in solar relative proportions over a wide range of metallicity and stellar mass (Woosley & Weaver 1995; Chieffi & Limongi 2004). Furthermore, measurements of Zn and Fe in Galactic halo stars with [Fe/H] $\gtrsim -2.0$ have shown that Zn/Fe accurately traces the solar ratio (Saito et al. 2009). For these reasons, we propose that the combination of [Si/Fe] at the lowest metallicities and [S/Zn] at the highest metallicities provides the most reliable diagnostic of the chemical evolution of α-capture and Fe-peak elements in DLAs, when drawing comparisons with Galactic halo stars.

Figure 3 shows the distribution of [α/Fe] values in DLAs in 0.25 dex wide bins of "metallicity" over nearly four orders of magnitude in [Fe/H], from [Fe/H] $= -3.75$ to 0.0, together with the standard deviation appropriate to each bin (represented by the error bars). To account for the uncertainty in both [α/Fe] and [Fe/H], we generated 1000 Monte Carlo realizations of each measurement prior to binning. Therefore, there is a small amount of correlation between neighboring symbols. Red symbols denote values of [S/Zn] and [Zn/H] (as proxies for [α/Fe] and [Fe/H], respectively) from the compilation of such measurements by Vladilo et al. (2011), while the blue circles correspond to the values of [Si/Fe] and [Fe/H] collected in Table 1. Both sets of data are constructed exclusively from measurements using spectra of high signal-to-noise ratio (S/N) and resolution. Note the good agreement between red and blue symbols near [Fe/H] $\simeq -2.0$, where the two data sets overlap.

Also shown in Figure 3 are equivalent data for Galactic halo stars (gray circles; Venn et al. 2004). In this case, the [α/Fe] values were calculated from the average of the ratios Mg/Fe, Si/Fe, and Ca/Fe, depending on the data available for a particular star. This is in line with many previous stellar studies, and is supported by the results of nucleosynthesis calculations showing that the relative yields of Mg, Si, S, and Ca from massive stars are in solar relative proportions when integrated over a Salpeter-like stellar IMF (Woosley & Weaver 1995; Chieffi & Limongi 2004).

In order to demonstrate that a typical DLA experiences a different SFH to the galaxies that built the MW stellar halo, we perform a proof by contradiction, with the starting hypothesis that a typical DLA experiences an identical SFH as the galaxies that predominantly built the stellar halo of the MW. Under this hypothesis, we are justified in our assumption that [S/Si] $= 0.0$ and [Zn/Fe] $= 0.0$ for [Fe/H] $\gtrsim -2.5$. As can be appreciated from the comparison presented in Figure 3, halo stars and DLAs agree in exhibiting an [α/Fe] $\simeq +0.3$ plateau when [Fe/H] $\lesssim -2.0$, as noted previously by Rafelski et al. (2012). A similar plateau is also observed in oxygen: [O/Fe] $\simeq +0.4$ in DLAs with [Fe/H] $\lesssim -2.0$ (Cooke et al. 2011b). These plateaux represent the enhanced [α/Fe] level set by massive stars.[9] However, for metallicities [Fe/H] $\gtrsim -2.0$, the DLA population exhibits a gentle decline in [α/Fe] toward solar values, presumably marking an increased contribution of Fe-peak elements from Type Ia SNe. In this aspect, DLAs are clearly different from Galactic halo stars which *maintain* an approximately constant α-enhancement from [Fe/H] $= -3.75$ to [Fe/H] ~ -0.75. This disagreement contradicts our initial hypothesis, therefore implying that a *typical* DLA experienced a different chemical enrichment history from that of the MW stellar halo.

[8] It is well established that in DLAs the first ions are the dominant stages of the corresponding elements. Notable exceptions are N and O, which are predominantly neutral (see Morton et al. 1973, and Section 5.2 below).

[9] The different levels of these plateaux at low metallicities, corresponding to [O/Si] $\simeq +0.1$, are in good agreement with low-metallicity nucleosynthesis calculations (Woosley & Weaver 1995; Chieffi & Limongi 2004; Heger & Woosley 2010).

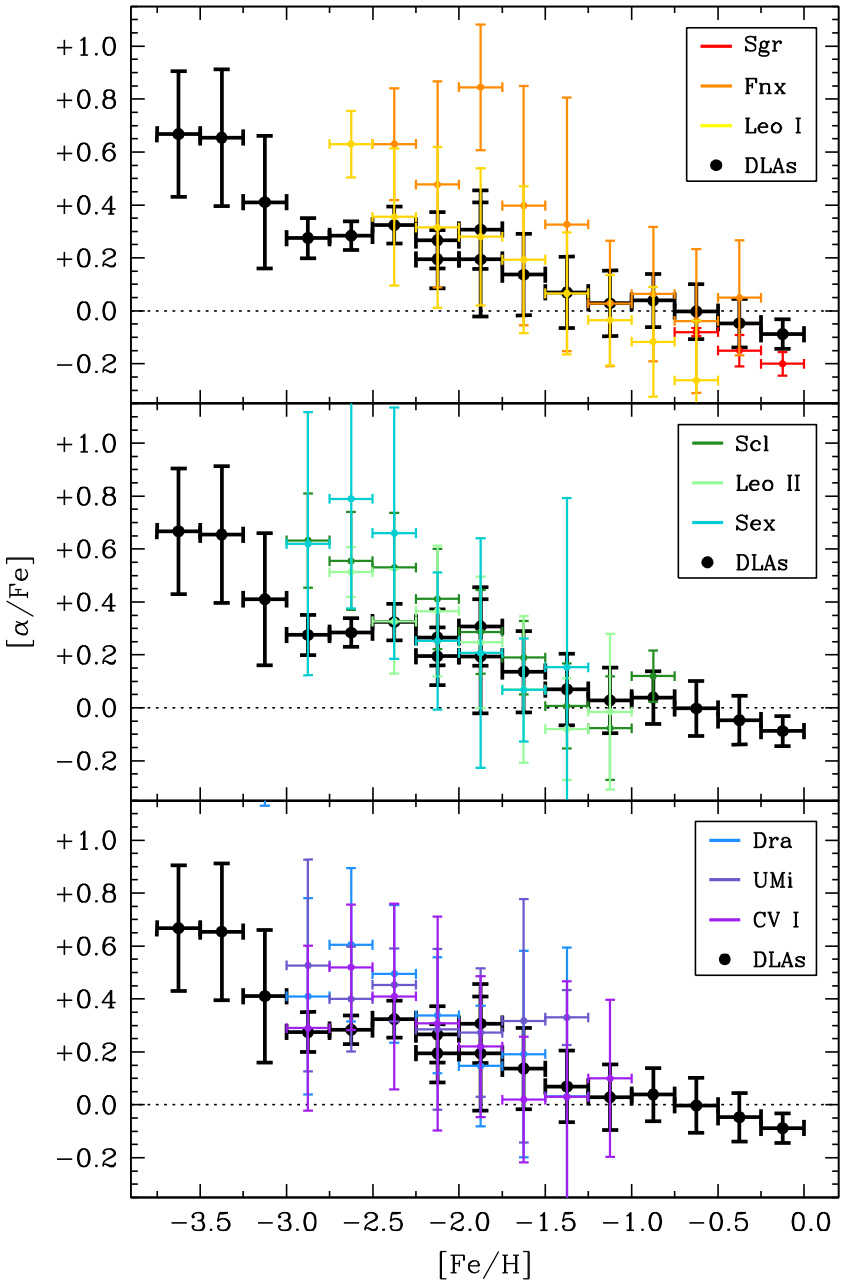

Figure 4. [α/Fe] ratio in DLAs (black symbols; cf. Figure 3) are compared to the typical [α/Fe] measured in the classical Milky Way satellite dwarf galaxies. For clarity, the dSph galaxies are color-coded by their *V*-band absolute magnitude, where red represents the brightest dSph (Sgr) and purple represents the faintest dSph (CV I). The data for Sgr are taken from Bonifacio et al. (2004), Monaco et al. (2005), and Sbordone et al. (2007). The data for the remaining dSphs are from Kirby et al. (2011a).

Rather, the dependence of the α/Fe ratio on metallicity in high-redshift DLAs seems to be more akin to that seen in local dSph galaxies (Kirby et al. 2011a), as can be realized by considering Figure 4. For clarity, we have divided the dSph into three subsets, as indicated; in each of the three panels we show the same set of DLA measurements as in Figure 3, now uniformly indicated by black symbols, assuming that [Zn/Fe] = 0. In general, there appears to be much in common between the chemical evolutions of MW dSph galaxies on the one hand and of DLAs at redshift $z_{\rm abs} \sim$ 2–3 on the other (we investigate our assumption that [Zn/Fe] = 0 for dSph stars directly below). We also note a similarity in the DLA measures of [α/Fe] and [Fe/H] to those recently determined in the dwarf galaxies associated with M31, in particular AndV (see Figure 4 of Vargas et al. 2014).

Regarding the MW systems, there may be some tension toward the lowest metallicities, where dSph stars are somewhat more α-enhanced relative to the DLAs. This could be the result of small number statistics, modeling techniques, or genuine differences between DLAs and the dSphs. We note that several studies working with many fewer stars than Kirby et al. (2011a), but with somewhat higher S/N and resolution, have reported an [α/Fe] plateau for low-metallicity stars in some dSph galaxies at a level that is consistent with that seen in DLAs. Some examples include Fornax (Hendricks et al. 2014), Sculptor (Starkenburg et al. 2013; Hill & DART Collaboration 2012), and Ursa Minor (Cohen & Huang 2010). We also note that our comparison between DLAs and dSph galaxies for metallicities [Fe/H] $\gtrsim -2.0$ assumes that S traces Si whilst Zn follows Fe. As argued earlier, S and Si are believed to be produced in solar

relative proportions by massive stars, independent of chemical evolution. However, Zn may not always follow Fe in the dSph galaxies; unlike the stars in the MW disk and halo (Saito et al. 2009), the small number of measurements of [Zn/Fe] available in a few dSph galaxies suggests that [Zn/Fe] might vary with metallicity. Specifically, [Zn/Fe] = 0.0 near [Fe/H] = −2.0 for dSph galaxies, and gradually decreases to [Zn/Fe] $\simeq$ −0.2 to −0.5 near [Fe/H] = −1.0 (Shetrone et al. 2001; Sbordone et al. 2007; Cohen & Huang 2009, 2010). This difference between the dSph galaxies and the MW halo stars is likely due to their different SFH.[10] Therefore, to enable a fair comparison between DLAs and dwarf galaxies one should shift the DLA points to somewhat lower [α/Fe] and higher [Fe/H] values when [Fe/H] $\gtrsim$ −2.0. Thus, if the chemical evolution of a typical DLA is similar to that of a dwarf galaxy, such that [Zn/Fe] becomes subsolar for [Fe/H] $\gtrsim$ −2.0, the DLA "knee" will become even more pronounced.

With these reservations in mind, the similarity in the behavior of [α/Fe] as a function of [Fe/H] in DLAs and dSph galaxies displayed in Figure 4 in the metallicity range −2.0 $\leqslant$ [Fe/H] $\leqslant$ −1.0 suggests that the chemical evolution of a typical DLA ([Fe/H] $\simeq$ −1.5) is more akin to that of a dwarf galaxy than the MW. This similarity between the [α/Fe] abundance of DLAs and the MW dSph galaxies was also pointed out by Bonifacio et al. (2004), albeit with many fewer dSph stars and DLAs than in the present study. Our combined sample of 54 DLAs with reliable [α/Fe] measurements covering over three decades in metallicity has allowed us to trace the all-important "knee" in the [α/Fe] ratio. Of course, it is difficult to draw firm conclusions about the entire DLA population; for example, the high-metallicity DLAs considered in Figure 4 are unlikely to evolve as dwarf galaxies. Nevertheless, these data support a picture where a *typical* DLA likely traces the chemical evolution of a dwarf galaxy. Therefore, by extension, the most metal-poor DLAs likely represent the least chemically evolved dwarf galaxies at redshifts $z \sim 3$ that still have the potential to form stars. Future, more extensive measurements of S and Zn in dSph stars and low-metallicity DLAs would allow us to test this picture further.

5. THE PHYSICAL PROPERTIES OF METAL-POOR DLAs

As explained in the Introduction, the most metal-poor DLAs offer a rare opportunity to study the physical conditions of neutral gas in the metal-poor regime. Such conditions may provide important clues to better understand the physics of star formation in the lowest mass dwarf galaxies at early times. In this section, we consider some of the key physical parameters that can be deduced from the analysis of the absorption lines from the metal-poor DLAs in our sample. While there have been previous studies of this kind (e.g., Srianand et al. 2005; Wolfe et al. 2003), none so far have focused specifically on very metal-poor DLAs.

Our analysis starts with the determination of the kinetic temperature of the gas. As explained below, this is only possible for a subset of the metal-poor DLAs in Table 1. Specifically, only in nine out of the 23 DLAs in our sample, can the thermal (i.e., microscopic) contribution to the line broadening be reliably separated from the turbulent (i.e., macroscopic) broadening; in the other 14 cases either turbulent broadening completely dominates or there is insufficient information in the profiles of the absorption lines covered to decouple the two. This inevitably introduces a bias: The physical properties we deduce below apply to the relatively quiescent DLAs in our survey, and may not be fully representative of, for example, DLAs of a given metallicity. Despite this bias, however, the analysis is still worthwhile, given how little is known at present about some of the most basic physical properties of the most metal-poor DLAs. The sample considered in this section consists of 12 absorption components in nine DLAs whose relevant parameters are collected in Table 2. Formally, the absorption system at $z_{\rm abs} = 2.536509$ toward HS 0105+1619 is a sub-DLA, exhibiting a total H I column density less than the DLA threshold of $10^{20.3}$ H I atoms cm^{-2}. We nevertheless include this system in our sample of DLAs, as it provides a useful indication of the physical properties of neutral gas at somewhat lower H I column density.

For several DLAs, we report the H I column density of individual components. In these rare cases, we have detected multiple neutral deuterium lines. By assuming that each absorption component in these systems has an identical D/H ratio (Cooke et al. 2014), we have derived the H I column density of each component.

5.1. Measured Physical Quantities

DLA absorption line profiles are characterized by a Doppler width for the line broadening, a column density of each absorbing ion, and a redshift. The Doppler broadening further consists of a turbulent and a thermal component, specifically:

$$b^2 = b_{\rm turb}^2 + \frac{2\,k_{\rm B}\,T_{\rm gas}}{m_{\rm ion}}, \quad (1)$$

where $k_{\rm B}$ is the Boltzmann constant, $T_{\rm gas}$ is the gas kinetic temperature, and $m_{\rm ion}$ is the mass of the ion giving rise to an absorption line. Thus, by considering the absorption lines from multiple ions of widely differing mass, one can decouple the relative contributions of turbulent and thermal broadening (see Appendix A for further details).

In Columns 4 and 5 of Table 2, we list the derived turbulent Doppler parameters and kinetic temperatures in the 12 absorption components of the nine very metal-poor DLAs where this decoupling is possible. For completeness, we also provide the measured H I column density in each component and the corresponding chemical abundances. Our sample contains absorption systems with a range of H I column densities ($19.41 \leqslant \log N({\rm H\,I})/{\rm cm}^{-2} \leqslant 20.43$) and metallicities ($-2.64 \leqslant [{\rm O/H}] \leqslant -1.47$). In Figure 5, we show the distributions of turbulence parameter $b_{\rm turb}$ and of gas kinetic temperature $T_{\rm gas}$. The weighted mean values and 1σ dispersion for this sample are $\langle b_{\rm turb}\rangle = 3.5 \pm 1.1\,{\rm km\,s^{-1}}$ and $\langle T_{\rm gas}\rangle = 9800 \pm 1200\,{\rm K}$, respectively. Despite covering an order of magnitude in both metallicity and H I column density, we found no discernible correlations of the gas turbulence or temperature with either of these parameters.

The mean values of $b_{\rm turb}$ and $T_{\rm gas}$ reported here for metal-poor DLAs are not dissimilar to those typical of the so-called warm neutral medium (WNM) component of the MW ISM today (Wolfire et al. 1995, 2003), although the temperatures listed in Table 2 tend to be at the upper end of the values found locally. This broad similarity is perhaps surprising, given the difference by 2–3 orders of magnitude in metallicity between the high-z DLAs and the present-day Galactic ISM, and the attendant

[10] We also note that [Zn/Fe] is typically solar or subsolar when [Fe/H] > −2.0 in every galaxy observed locally, all of which exhibit a range of star formation histories. The supersolar [Zn/Fe] abundance that is commonly observed in DLAs is due to Fe being depleted onto dust grains (see, e.g., Rafelski et al. 2012).

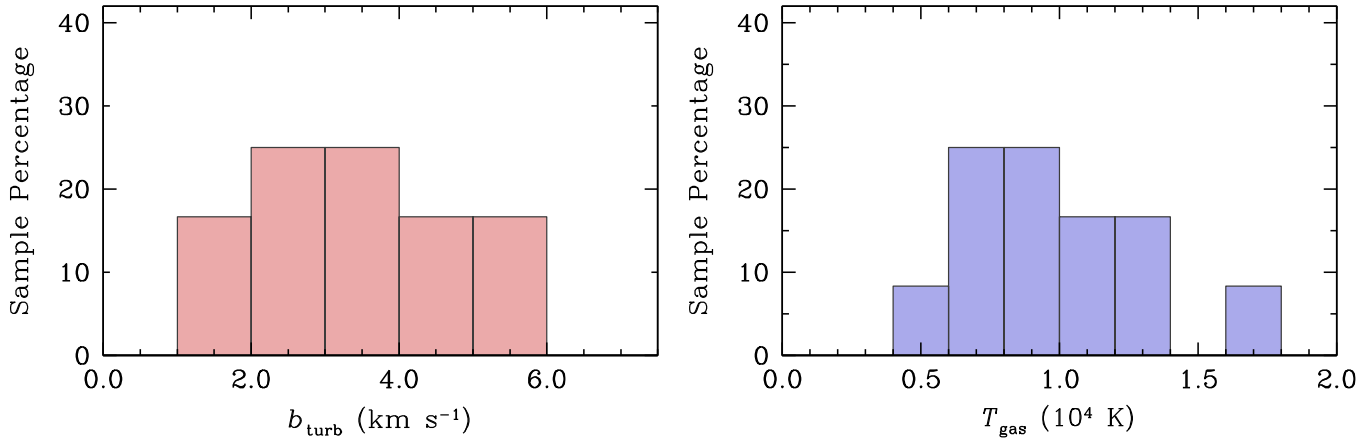

Figure 5. Distribution of the measured turbulent Doppler parameters (left panel) and gas kinetic temperatures (right panel) for a subset of our metal-poor DLA sample where the turbulent and thermal broadening of the absorption line profiles could be decoupled.

Table 2
Measured Physical Properties of Metal-poor DLAs[a]

QSO Name	$z_{\rm em}$	$z_{\rm abs}$	$b_{\rm turb}$ (km s^{-1})	$T_{\rm gas}$ [b] (K)	log $\frac{N({\rm H\,I})}{\rm cm^{-2}}$ [c]	log $\frac{N({\rm H\,I})}{\rm cm^{-2}}$ [d]	[O/H][e]	[Fe/H][e]	[Si/Fe][e]
J0035−0918	2.420	2.340097	1.1	7800	20.43	20.43	−2.44	−2.94	+0.37
		±0.000001	±0.4	±1600	±0.04	±0.04	±0.07	±0.06	±0.07
HS 0105+1619	2.652	2.536509	3.0	10800	19.415	19.426	−1.76	−2.10	+0.25
		±0.000001	±0.1	±200	±0.007	±0.006	±0.02	±0.05	±0.06
Q0913+072	2.785	2.618435	4.5	8400	20.09		−2.44	−2.73	+0.28
(comp. A)		±0.000001	±0.2	±1300	±0.02	20.312	±0.03	±0.02	±0.02
Q0913+072		2.618289	3.9	7700	19.84	±0.008	−2.35	−2.85	+0.29
(comp. B)		±0.000001	±0.2	±200	±0.03		±0.02	±0.04	±0.02
J1001+0343	3.198	3.078404	4.6	17000	20.21	20.21	−2.64	−3.48	+0.62
		±0.000002	±0.7	±8000	±0.05	±0.05	±0.06	±0.27	±0.27
J1111+1332	2.420	2.270940	2.2	13000	20.39	20.39	−1.92	−2.27	+0.32
		±0.000001	±0.1	±2000	±0.04	±0.04	±0.08	±0.04	±0.02
J1358+6522	3.173	3.0672594	2.4	5600	20.22	20.495	−2.06	−2.60	+0.31
		±0.0000005	±0.5	±1100	±0.06	±0.008	±0.06	±0.07	±0.03
J1419+0829	3.030	3.049654	2.8	9700	19.93		−1.82	−2.17	+0.23
(comp. A)		±0.000001	±0.2	±100	±0.02	20.392	±0.03	±0.04	±0.03
J1419+0829		3.049843	5.3	11600	20.209	±0.003	−1.99	−2.37	+0.24
(comp. B)		±0.000001	±0.2	±200	±0.008		±0.01	±0.03	±0.03
J1558−0031	2.823	2.702318	3.7	7200	20.27		−1.52	−1.90	+0.22
(comp. A)		±0.000003	±0.2	±1000	±0.08	20.75	±0.09	±0.08	±0.04
J1558−0031		2.702422	1.5	9300	20.29	±0.03	−1.47	−1.81	+0.28
(comp. B)		±0.000002	±0.3	±900	±0.11		±0.12	±0.11	±0.07
Q2206−199[f]	2.559	2.076229	5.3	12200	20.43	20.43	−2.04	−2.55	+0.30
		±0.000001	±0.2	±3000	±0.04	±0.04	±0.06	±0.04	±0.02

Notes.
[a] The DLAs in this table are a subset of our full sample (see Section 5).
[b] Our technique implicitly assumes that the gas is distributed according to a Maxwell–Boltzmann distribution. The uncertainty of the kinetic temperature measurements reported here only reflect the random uncertainty based on the statistical fluctuations in the data.
[c] H I column density for a given absorption component of the DLA.
[d] Total H I column density of the DLA.
[e] We have assumed a solar abundance of 12+log(O/H)$_\odot$ = 8.69, 12+log(Si/H)$_\odot$ = 7.51, 12+log(Fe/H)$_\odot$ = 7.47 (Asplund et al. 2009).
[f] Values are derived from Pettini et al. (2008) and Carswell et al. (2012).

differences in the dust-to-gas ratio and in the abundance of molecules (Petitjean et al. 2000). Furthermore, the DLA gas is likely to be exposed to a radiation field which is different in both shape and intensity from that irradiating local interstellar clouds. These are all factors that regulate the heating and cooling balance of the ISM; thus, the similarities found here between high-z metal-poor DLAs and the local WNM warrant a re-examination of two-phase models of the ISM under the conditions that apply at $z = 2$–3.

Only a small number of studies have previously attempted to measure the temperature of DLA gas at high-redshift. In a few favorable cases, a curve-of-growth analysis has been used to estimate the Doppler broadening of unresolved absorption lines from molecular or neutral metal absorption lines (Jorgenson et al. 2009; Tumlinson et al. 2010). In both of these studies, the temperature of the gas was measured to be a few 100 K or less, consistent with the typical values estimated for the "cold neutral medium" (CNM) of the MW ISM. Other investigations

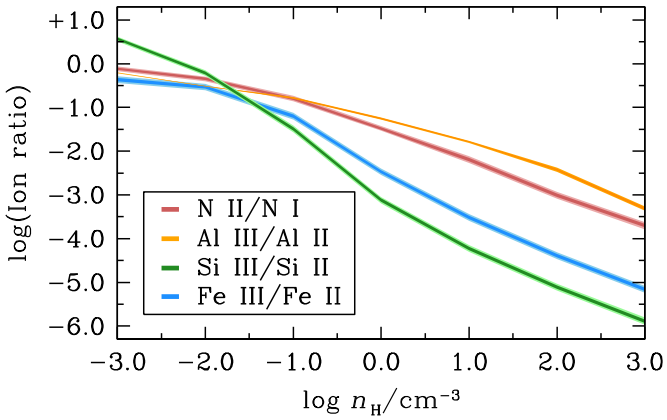

Figure 6. Solid curves show the results of our *Cloudy* simulations of a metal-poor DLA irradiated by the Haardt & Madau (2012) UV background. This example calculation is for J0035−0918 (see Appendix B), which has $\log N(\mathrm{Si\,II})/N(\mathrm{Si\,II}) = -1.08 \pm 0.33$, and $\log N(\mathrm{N\,II})/N(\mathrm{N\,I}) \leqslant -0.62$ (3σ). The corresponding estimates of the H volume density based on these calculations are $\log n_\mathrm{H}/\mathrm{cm}^{-3} = -1.3 \pm 0.3$ and $\geqslant -1.4$, respectively.

have instead used the relative strengths of the fine-structure states of C and Si to estimate the DLA gas kinetic temperature (Howk et al. 2005; Jorgenson et al. 2010). These authors also report temperatures less than a few 100 K. A conclusion that is emphasized by all of the above studies is that the absorption from molecules, neutral species, and the fine structure states provide a probe of the physical properties of the CNM. In our work, we have directly measured the kinetic temperature of the H I gas associated with the first ions, and have found that this DLA gas is much warmer than the CNM and is consistent with a WNM (see also Carswell et al. 2012).

5.2. Derived Physical Quantities

Temperature, turbulence, neutral gas column density, and chemical composition are all parameters that can be measured directly from the absorption lines in our spectra. Armed with this information, we can also deduce several other physical properties relevant to metal-poor DLAs.

To this end, we have performed a suite of *Cloudy* photoionization simulations (Ferland et al. 2013). We model each DLA in our sample as a constant density plane-parallel slab of gas irradiated by the Haardt & Madau (2012) extragalactic background and the cosmic microwave background at the appropriate redshift. We consider a uniform grid of H volume densities in the range $-3.0 \leqslant \log n_\mathrm{H}/\mathrm{cm}^{-3} \leqslant +3.0$, with a cosmic abundance of He (i.e., $n_\mathrm{He}/n_\mathrm{H} = 1/12$) and globally scale the metal abundance of the slab to the [Si/H] abundance derived for each DLA.[11] The calculations are stopped when the H I column density of the slab is equal to that of the DLA, and a selection of metal ion column densities are output. We perform 1000 Monte Carlo realizations of the above slab, each time drawing a new value for the stopping H I column density from the observed value and its associated error. The results from an example calculation are shown in Figure 6, where, for an assumed radiation field, the column density ratio of successive ion stages of a given element is sensitive to the H volume density of the gas, $n(\mathrm{H})$.[12]

[11] Quantitatively indistinguishable results were found when we considered a modest α-enhancement.

[12] We also used these simulations to confirm that ionization corrections to the absolute metal abundances of the DLAs listed in Table 2 are <0.1 dex (see also Cooke et al. 2011b). For the sub-DLA HS 0105+1619 the *absolute* metallicity correction is −0.2 dex; however, the ionization corrections for the *relative* metal abundance of the first ions are <0.05 dex.

In metal-poor DLAs, the most commonly observed ion ratios include N II/N I, Al III/Al II, Si III/Si II, and Fe III/Fe II. As can be seen from Figure 6, the most sensitive probe of the H volume density is the Si III/Si II ratio. Which of the four ion ratios is available in a given DLA depends on redshift, metallicity, column density, and blending with other absorption lines. In cases where more than one ion ratio is covered, the values of n_H deduced are generally in good mutual agreement. Column 4 of Table 3 lists the values of DLA volume density so derived; $n_\mathrm{H} \sim 0.1$ cm^{-3} seems typical.

With these values of n_H, we can straightforwardly calculate the mass density of each DLA

$$\rho_\mathrm{gas} = 1.33\, m_\mathrm{p}\, n_\mathrm{H}, \tag{2}$$

where m_p is the mass of an H atom, and the factor 1.33 accounts for He.

Using the measured kinetic temperature and turbulence of the DLAs, together with our determinations of the number and mass densities of the gas, the thermal and turbulent gas pressures are respectively given by

$$P_\mathrm{th} = (n_\mathrm{H} + n_\mathrm{He})\, k_\mathrm{B}\, T_\mathrm{gas} \simeq 1.083\, n_\mathrm{H}\, k_\mathrm{B}\, T_\mathrm{gas} \tag{3}$$

and

$$P_\mathrm{turb} = \frac{\rho_\mathrm{gas}\, \langle v^2 \rangle}{2} = \frac{3 \rho_\mathrm{gas}\, b_\mathrm{turb}^2}{4}. \tag{4}$$

We can also convert our measure of the kinetic temperature of the gas into the sound speed of the gas

$$c_\mathrm{s} = \sqrt{\frac{P_\mathrm{th}}{\rho_\mathrm{gas}}} = \sqrt{\frac{k_\mathrm{B}\, T_\mathrm{gas}}{1.23\, m_\mathrm{p}}} \tag{5}$$

from which we can calculate the turbulent Mach number

$$\mathcal{M}_\mathrm{turb} = \frac{\sqrt{\langle v^2 \rangle}}{c_s} = \frac{\sqrt{3/2}\, b_\mathrm{turb}}{c_\mathrm{s}}. \tag{6}$$

Note that Equations (5) and (6) are simply conversions of measured physical quantities, and therefore do not depend on the density derived from our *Cloudy* simulations.

The cloud size (along the line of sight) is obtained directly from the ratio of the column density of H I and the total H volume density:

$$L_\mathrm{HI} = \frac{N(\mathrm{H\,I})}{n_\mathrm{H}}, \tag{7}$$

where we have assumed that $n_\mathrm{H\,I} \simeq n_\mathrm{H}$. Our *Cloudy* simulations justify this assumption, since the neutral H volume density is $n_\mathrm{H\,I} \gtrsim 0.9\, n_\mathrm{H}$ for gas seen in absorption as a DLA.

In order to proceed further, we need to make an assumption about the geometry of the absorbers. One possibility is that, by selecting for analysis the DLAs with the lowest turbulent velocities, we preferentially pick out face-on disks. In such cases, it is hard to extrapolate from the parameters measured along our lines of sight to the global properties of the disk galaxy intersected. On the other hand, if the gas distribution is not highly flattened, then our data may be more representative of the DLA host as a whole. Thus, it is instructive to consider the implications of our measurements for the case of a spherical geometry of the absorber.

If the gas is spherically distributed, and our line of sight is close to the maximum projected H I column density, then the radius of these clouds is approximately given by $r_\mathrm{H\,I} = L_\mathrm{H\,I}/2$.

Table 3
Derived Physical Properties of Metal-poor DLAs[a]

QSO Name	z_{em}	z_{abs}	$\log n_H$ (cm^{-3})	$r_{H\,I}$ (pc)	M_{WNM} ($10^5\,M_\odot$)	P_{th}/k_B (K cm^{-3})	P_{turb}/k_B (K cm^{-3})	c_s (km s^{-1})	$\mathcal{M}_{turb}$
J0035−0918	2.420	2.340097	-1.3 ± 0.3	1270^{+930}_{-610}	220^{+360}_{-160}	700^{+730}_{-360}	17^{+24}_{-10}	$7.2^{+0.7}_{-0.8}$	$0.19^{+0.07}_{-0.07}$
HS 0105+1619	2.652	2.536509	-0.8 ± 0.3	43^{+42}_{-21}	$\leqslant 0.4$	2790^{+2250}_{-1350}	270^{+250}_{-130}	$8.51^{+0.08}_{-0.08}$	$0.43^{+0.02}_{-0.02}$
Q0913+072 (comp. A)	2.785	2.618435	-0.9 ± 0.2	200^{+120}_{-70}	$1.6^{+2.5}_{-1.0}$	1440^{+890}_{-550}	380^{+210}_{-140}	$7.5^{+0.6}_{-0.6}$	$0.73^{+0.07}_{-0.06}$
Q0913+072 (comp. B)		2.618289	-1.12 ± 0.05	150^{+20}_{-20}	$0.37^{+0.13}_{-0.10}$	640^{+80}_{-70}	140^{+20}_{-20}	$7.19^{+0.09}_{-0.09}$	$0.66^{+0.04}_{-0.04}$
J1001+0343	3.198	3.078404	$\geqslant -1.7$	$\leqslant 1320$	$\leqslant 63$	$\geqslant 370$	$\geqslant 50$	$10.7^{+2.2}_{-2.8}$	$0.52^{+0.17}_{-0.11}$
J1111+1332	2.420	2.270940	-1.2 ± 0.3	1080^{+890}_{-530}	180^{+340}_{-130}	1440^{+1440}_{-730}	56^{+58}_{-28}	$9.3^{+0.7}_{-0.7}$	$0.28^{+0.04}_{-0.03}$
J1358+6522	3.173	3.0672594	-0.93 ± 0.05	240^{+50}_{-40}	$2.4^{+1.5}_{-0.9}$	750^{+170}_{-160}	100^{+40}_{-30}	$6.1^{+0.6}_{-0.6}$	$0.48^{+0.12}_{-0.11}$
J1419+0829[b] (comp. A)	3.030	3.049654	-0.35 ± 0.08	32^{+7}_{-6}	$0.021^{+0.010}_{-0.007}$	4850^{+970}_{-820}	450^{+120}_{-90}	$8.07^{+0.04}_{-0.04}$	$0.43^{+0.03}_{-0.03}$
J1419+0829[b] (comp. B)		3.049843	$\geqslant -1.20$	$\leqslant 420$	$\leqslant 6.2$	$\geqslant 790$	$\geqslant 210$	$8.82^{+0.08}_{-0.08}$	$0.74^{+0.03}_{-0.03}$
J1558−0031 (comp. A)	2.823	2.702318	-0.53 ± 0.11	110^{+40}_{-30}	$0.76^{+0.85}_{-0.40}$	2480^{+820}_{-630}	520^{+160}_{-130}	$6.9^{+0.5}_{-0.5}$	$0.65^{+0.06}_{-0.05}$
J1558−0031 (comp. B)		2.702422	-1.17 ± 0.20	620^{+420}_{-250}	39^{+90}_{-27}	850^{+510}_{-320}	26^{+20}_{-12}	$7.9^{+0.4}_{-0.4}$	$0.23^{+0.05}_{-0.05}$
Q2206−199	2.559	2.076229	$\geqslant -1.6$	$\leqslant 1700$	$\leqslant 170$	$\geqslant 330$	$\geqslant 90$	$9.0^{+1.1}_{-1.2}$	$0.72^{+0.11}_{-0.08}$

Notes. Quoted errors are 1σ confidence intervals. Note that the probability distributions show a high degree of asymmetry.
[a] The DLAs in this table are a subset of our full sample (see Section 5). The table columns have the following meaning: Columns 1 and 2: quasar name and redshift; Column 3: absorption redshift of the intervening DLA; Column 4: logarithmic volume number density of the DLA gas; Columns 5 and 6: radial extent and total mass of the DLA's neutral gas; Columns 7 and 8: thermal and turbulent pressure of the gas in units of the Boltzmann constant; Columns 9 and 10: sound speed and turbulent Mach number of the DLA gas.
[b] We caution the reader that this system is a "proximate" DLA, with $z_{abs} \simeq z_{em}$. Our *Cloudy* modeling does not include the radiation field from the QSO; the effect of the QSO depends on the unknown distance between it and the DLA. If the QSO's radiation field contributes significantly, n_H for Component A should be considered as an upper limit, whereas n_H for Component B would be unconstrained by the present models.

As can be seen from Column 5 of Table 3, the radii of the DLAs sampled are typically less than 1 kpc and range from ∼30 to ∼1300 pc. Radius and density together give the total mass of warm neutral gas (again, assuming a spherical geometry):

$$M_{WNM} = \rho_{gas} \times \frac{4\pi}{3} r_{H\,I}^3, \quad (8)$$

which is a lower limit if the quasar line of sight does not pass through the center of the metal-poor DLA. All of the quantities derived above are listed in Table 3.

5.3. The Physical Properties of Near-pristine Neutral Gas

The physical properties that we have derived provide new insights into the nature of metal-poor DLAs and of star formation in the lowest metallicity environments. We first investigate the relationship between the kinetic temperature and H volume density, illustrated in Figure 7. We divide our sample equally in two, and color code the symbols according to their [O/H] metallicity; blue symbols represent the relatively metal-poorer sub-sample (with [O/H] $\lesssim -2.0$), while the red symbols are for the relatively metal-richer sub-sample (with [O/H] $\gtrsim -2.0$). In Figure 7, we have also drawn a series of solid lines of constant pressure (P_{th}/k_B) in the T_{gas}–n_H plane. Although the sample size is still small, these data suggest that metal-richer DLAs have a slight preference to host gas that is at modestly higher densities and temperatures, and therefore higher pressures, compared with the metal-poorer sample.

We note that the majority of the DLAs in our sample are at lower pressures than the mean $P_{th}/k_B \simeq 3000$ K cm^{-3} determined by Jenkins & Tripp (2001, 2011) for diffuse interstellar clouds within a few kpc of the Sun. Pressures in metal-poor DLAs are also significantly lower than those typical of DLAs with detectable column densities of molecular hydrogen, which tend to be at the metal-rich end of the distribution of DLA metallicities (Srianand et al. 2005).

By inspection of the thermal and turbulent pressures listed in Table 3, we can also conclude that the most metal-poor DLAs are predominantly held up by thermal pressure, as is the case for

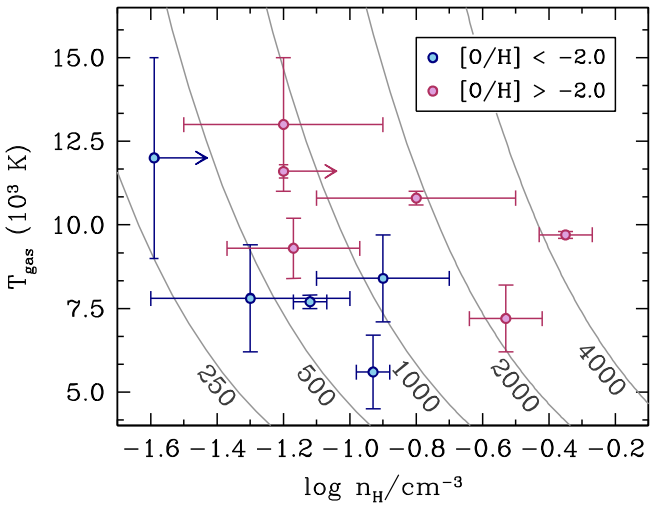

Figure 7. Relationship between the kinetic temperature T_{gas} and the H volume density n_H of metal-poor DLAs. We have divided our sample equally into a metal-richer (with [O/H] $\gtrsim -2.0$; red points) and a metal-poorer sub-sample (with [O/H] $\lesssim -2.0$; blue points). From this comparison, it is apparent that the relatively metal-richer DLAs favor somewhat higher temperatures and densities compared with the metal-poorer DLAs. The gray solid curves indicate lines of constant pressure, labeled in units of P_{th}/k_B. For comparison, the mean thermal pressure of the neutral ISM near the Sun is $P_{th}/k_B \simeq 3000$ K cm^{-3}.

the WNM in the local ISM (Vallerga 1996; Redfield & Linsky 2004). Similarly, the turbulent Mach number that we derive for the DLAs in our sample ($\mathcal{M}_{\rm turb} \sim 0.5$) is reminiscent of the local ISM values; every DLA that we have analyzed here exhibits a subsonic turbulent Mach number. Such low Mach numbers suggest that the WNM in the most metal-poor DLAs follows a fairly smooth gas density distribution (Kowal et al. 2007; McKee & Ostriker 2007), which is not conducive to gas fragmentation. Presumably, star formation in the most metal-poor DLAs proceeds via a CNM that, based on local studies (e.g., Heiles & Troland 2003), would exhibit a supersonic $M_{\rm turb}$. The existence of a two-phase medium with a cold and warm component is supported by H I 21 cm observations of neutral gas in Leo T and Leo P—two nearby low-metallicity dwarf galaxies in the Local Group (Ryan-Weber et al. 2008; Bernstein-Cooper et al. 2014).

Such observations have not yet been conducted on redshift $z \sim 3$ very metal-poor DLAs. However, there exists a handful of 21 cm absorption measurements for DLAs in front of radio-bright quasars (Srianand et al. 2012; Kanekar et al. 2014). In this case, the optical depth of 21 cm absorption depends on the H I column density, the spin temperature, and a covering factor that describes how effectively the foreground DLA covers the extended radio emission of the background quasar. For gas in a WNM, Liszt (2001) demonstrated that collisional excitation is unable to efficiently thermalize the H I λ21 cm line, leading to spin temperatures that are somewhat less than the kinetic temperature of the gas. A relationship between the spin and kinetic temperatures is further complicated by the uncertain fraction of gas along the line-of-sight that is in a CNM versus a WNM; a high CNM fraction weights the line-of-sight spin temperature toward lower values. In principle, the fewer coolants that are available in low-metallicity gas imply lower CNM fractions, and therefore higher spin temperatures; presumably this is the origin of the observed anti-correlation between spin temperature and metallicity (Kanekar & Chengalur 2001; Kanekar et al. 2014). By extrapolating the relationship between spin temperature and metallicity of the DLA population, the most metal-poor DLAs in our analysis presumably exhibit relatively high spin temperatures, corresponding to a low fraction of CNM gas.

For convenience, we provide a summary of the key physical properties of the most metal-poor DLAs in Table 4.[13] In brief, our observations and analysis suggest that the most metal-poor DLAs are clouds that typically contain a reservoir of $\sim 10^{4-7}\,M_{\odot}$ of warm neutral gas with a temperature $T_{\rm gas} \simeq 9600$ K. This gas is expected to have a smooth density distribution, and is predominantly supported by thermal pressure. Although our measurement technique is not sensitive to the presence or absence of a CNM (see Appendix A for details), we point out that the properties of the inferred WNM are not conducive to star formation. Given the absence of molecular absorption lines in our DLA sample, considered a tracer of the CNM, we suggest that a CNM could be present in these DLAs with either a small cross-sectional area, or may only exist for a relatively short phase of a DLA's life just prior to a burst of star formation. The absence of a CNM in our DLA sample is consistent with the paucity of strong molecular hydrogen absorption associated with the general DLA population (Jorgenson et al. 2014). In addition, metal-poor DLAs might contain very low CNM fractions, in agreement with recent cosmological hydrodynamic simulations (Maio et al. 2014).

Table 4
Summary of the Physical Properties of Metal-poor DLAs

Property	Confidence Intervals
$b_{\rm turb}$ (km s^{-1})	$3.3^{+1.8}_{-1.5}$ (1σ) $^{+2.3}_{-2.4}$ (2σ)
$T_{\rm gas}$ (K)	9600^{+2500}_{-2600} (1σ) $^{+12200}_{-5000}$ (2σ)
$\log n$(H)/cm^{-3}	$-1.0^{+0.4}_{-0.3}$ (1σ) $^{+0.6}_{-0.7}$ (2σ)
$r_{\rm H\,I}$ (pc)	220^{+840}_{-130} (1σ) $^{+2200}_{-200}$ (2σ)
$\log M_{\rm WNM}/M_{\odot}$	$5.4^{+1.9}_{-0.9}$ (1σ) $^{+2.5}_{-2.5}$ (2σ)
$P_{\rm th}/k_{\rm B}$ (K cm^{-3})	1050^{+1610}_{-450} (1σ) $^{+4150}_{-730}$ (2σ)
$P_{\rm turb}/k_{\rm B}$ (K cm^{-3})	130^{+330}_{-100} (1σ) $^{+630}_{-120}$ (2σ)
$c_{\rm s}$ (km s^{-1})	$8.0^{+1.0}_{-1.2}$ (1σ) $^{+4.1}_{-2.5}$ (2σ)
$\mathcal{M}_{\rm turb}$	$0.50^{+0.23}_{-0.24}$ (1σ) $^{+0.34}_{-0.36}$ (2σ)

6. METAL-POOR DLAs AND MODERN-DAY DWARF GALAXIES

In the previous sections, we have assessed the kinematic, chemical, and physical aspects of the metal-poor DLA population. With these observations, we can start building a connection between the metal-poor DLA population at high-redshifts and their modern-day counterparts which are presumably akin to Local Group dwarf galaxies (Salvadori & Ferrara 2012). In this section, we summarize what can be learnt by studying the lowest mass galaxies over cosmic time.

Detailed star formation histories that are extracted from CMDs of Local Group dwarf galaxies (Weisz et al. 2011, 2014a) imply that these galaxies formed a considerable fraction of their present-day stellar population between redshifts $z \sim 2$ and 5 (Weisz et al. 2014a), corresponding to the range of redshifts that are probed by our metal-poor DLA sample. Furthermore, the observed kinematics of the metal-poor DLA population show a similar trend to that observed in Local Group galaxies, where the systems with the lowest metallicities also exhibit the lowest velocity dispersions. From this observation, we propose that the most metal-poor DLAs are associated with the lowest mass halos that can potentially form stars at redshift $z \sim 3$.

This conclusion receives additional support from the observed chemical evolution of the DLA population. Specifically, the evolution of the α/Fe ratio with metallicity (as measured by Fe/H) for a typical DLA is broadly similar to that seen in the local, low-mass dwarf galaxies, and is clearly different from the behavior of this ratio in MW stars of the halo and thin and thick disks (Venn et al. 2004; Bensby et al. 2005). The chemical evolution of a typical DLA also differs, although to a lesser extent, in the dependence of the α/Fe ratio on metallicity compared to relatively massive dwarf galaxies, such as the Small and Large Magellanic Clouds (Hill et al. 1997; Venn 1999; Pompéia et al. 2008) and the Sagittarius dSph (de Boer et al. 2014). The observations presented herein suggest that the chemical evolution of a typical DLA is similar to galaxies that are somewhat less massive than the Magellanic Clouds. By extension, we propose that the most metal-poor DLAs at redshift $z \sim 3$ most likely represent the earliest stages of chemical evolution that were experienced by the lowest mass dwarf galaxies.

[13] For the physical properties that depend on the gas volume density, we found that the values changed by ~10% when we exclude the proximate DLA toward J1419+0829. In addition, we have found that the sub-DLA toward HS 0105+1619 has very similar properties to the DLA sample; the inclusion or exclusion of this sub-DLA has a negligible effect on the average properties listed in Table 4.

Of course, the observed $z \sim 3$ population of metal-poor DLAs need not represent the entire Local Group dwarf galaxy population. For example, some of the UFDs appear to have formed most of their stars prior to $z \sim 3$ (e.g., Hercules and Leo IV; Weisz et al. 2014a, 2014b). Indeed, some of the UFDs may have experienced "reionization quenching"(e.g., Bullock et al. 2000), and may therefore not be observable as gas-rich metal-poor DLAs at $z \sim 3$. Nevertheless, these near-pristine DLAs can still improve our understanding of the physical conditions for star formation in this low-metallicity regime.

Finally, consider the current working definition of a "first galaxy"—that is, in its simplest terms, a long-lived stellar population confined by a dark matter halo (see, e.g., the review by Bromm & Yoshida 2011). Using this definition, we suggest that the *most* metal-poor DLAs may trace a reservoir of largely primordial neutral gas that is confined to a dark matter halo yet to form its first long-lived stellar population. Indeed, some near-pristine DLAs may contain the hallmark chemical signatures of enrichment by metal-free Population III stars (Cooke et al. 2011a, the chemical abundance pattern of that DLA is updated herein—see Appendix B). It is therefore certainly plausible that some of the most metal-poor DLAs may not even fit the canonical definition of a "galaxy," until they form their second generation of stars.

7. SUMMARY AND CONCLUSIONS

In this paper, we have provided the first observational links between the local, well-studied population of dwarf galaxies and their most likely progenitors at high-redshift. Our study considers the kinematic, chemical, and physical properties of the metal-poor DLA population, which all favor the interpretation that such systems predominantly trace the early evolution of dwarf galaxies. From the sample of metal-poor DLAs considered here, we draw the following conclusions.

1. We measure the kinematics of a sample of 23 metal-poor DLAs with [Fe/H] $\lesssim -2.0$ and conclude that the most metal-poor systems are likely to be associated with the lowest mass galaxies that have the potential to form stars at redshift $z \sim 3$. We also find a close correspondence between our DLAs and the kinematics of Local Group dwarf galaxies of similar metallicities.
2. To better understand the chemical evolution of the whole DLA population, we have considered the variation in [α/Fe] of DLAs as a function of [Fe/H] metallicity. We find evidence for a "knee" in the evolution of [α/Fe] in DLAs at [Fe/H] $\simeq -2.0$, which is entirely consistent with the knee that is observed in most of the dSph galaxies near the MW (assuming [Zn/Fe] $\simeq 0$ when [Fe/H] $\simeq -2.0$, as supported by observations of dSphs). Conversely, the behavior of [α/Fe] versus [Fe/H] in the DLA population clearly differs from that exhibited by MW halo stars. We conclude that the $z \sim 3$ DLA population is not representative of galaxies similar to those that merged to form the bulk of the MW stellar halo.
3. We have examined the physical conditions of the gas giving rise to metal-poor DLAs, by compiling a sample of systems with the most well-determined cloud models where it is possible to decouple the turbulent and thermal broadening of the line profiles. From the analysis of nine metal-poor DLAs ([Fe/H] ~ -2.3) with a total of 12 cloud components, we estimate that the typical values of the turbulent Doppler parameter and of the gas kinetic temperature are $b_{\rm turb} = 3.3^{+1.8}_{-1.5}$ km s^{-1} and $T_{\rm gas} = 9600^{+2500}_{-2600}$ K, respectively.
4. Using *Cloudy* photoionization calculations, we have also estimated the gas density in each of the 12 DLA absorbers. Taken together, these measures have allowed us to estimate the mass, radial extent, thermal and turbulent pressure, and turbulent Mach number for these near-pristine clouds of neutral gas. We find that metal-poor DLAs contain roughly 10^{4-7} $M_\odot$ of neutral gas, and are predominantly supported by thermal pressure. Furthermore, all DLAs in our sample exhibit subsonic Mach numbers, which implies that the distribution of warm neutral gas in these systems is relatively smooth.

Our analysis has provided new insights into the nature of the most metal-poor DLAs, and the first glimpse into the physical conditions of star formation in low-metallicity gas at high-redshift. This now opens up the exciting prospect of studying in depth with future work the early evolution of galaxies analogous to the Local Group dwarfs, more than 10 billion years in the past, at a time when they were building the bulk of their present-day stellar populations.

We are grateful to the staff astronomers at the ESO VLT and Keck Observatory for their assistance with the observations. We thank the Hawaiian people for the opportunity to observe from Mauna Kea; without their hospitality, this work would not have been possible. We are thankful to an anonymous referee for a constructive and thorough report that improved the presentation of our work. We also wish to thank Tom Abel, Thomas de Boer, Mark Krumholz, Marc Rafelski, and Erik Tollerud for valuable discussions and comments. M. P. would like to thank Matteo Monelli and Stefania Salvadori for organizing the Symposium "Local Group, local cosmology" (EWASS 2013), which provided useful insights into some of the properties of Local Group dwarf galaxies. R.J.C. was partially supported by NSF grant AST-1109447 during this work, and is currently supported by NASA through Hubble Fellowship grant HST-HF-51338.001-A, awarded by the Space Telescope Science Institute, which is operated by the Association of Universities for Research in Astronomy, Inc., for NASA, under contract NAS5- 26555. R.A.J. gratefully acknowledges support from the NSF Astronomy and Astrophysics Postdoctoral Fellowship under award AST-1102683.

APPENDIX A
THERMAL AND TURBULENT BROADENING

The cloud models for all of the DLAs considered in this work were analyzed with the new Voigt profile fitting software recently developed for precision absorption line profile analysis (Cooke et al. 2014). This Absorption LIne Software (ALIS), uses a Levenberg–Marquardt chi-squared minimization algorithm to minimize the residuals between the data and the model, weighted by the error spectrum (e.g., Markwardt 2009). ALIS uses the atomic data compiled by Morton (2003), with updates from both Jenkins & Tripp (2006) and Murphy & Berengut (2014).

The absorption line profiles for the most metal-poor DLAs typically have a very low velocity dispersion, often with just a single narrow absorption line. In the present work, we have utilized the simplicity of the absorption line profiles exhibited by the most metal-poor DLAs to decouple the relative

Table 5
Ion Column Densities of the DLA in J0035−0918 at $z_{abs} = 2.340097$

Ion	Transitions Used	log N(X)/cm^{-2}	[X/H]	[X/Fe]
H I	1215	20.43 ± 0.04	...	...
C II	1036, 1334	14.50 ± 0.15	-2.36 ± 0.16	$+0.58 \pm 0.16$
N I	1134.1, 1134.4, 1134.9, 1199.5, 1200.2, 1200.7	13.37 ± 0.05	-2.89 ± 0.06	$+0.05 \pm 0.07$
N II	1084	$\leqslant 12.60$[a]	...	...
O I	971, 988, 1039, 1302	14.68 ± 0.06	-2.44 ± 0.07	$+0.50 \pm 0.08$
Al II	1670	11.68 ± 0.06	-3.19 ± 0.07	-0.25 ± 0.08
Si II	989, 1193, 1260, 1304, 1526	13.37 ± 0.05	-2.57 ± 0.06	$+0.37 \pm 0.07$
Si III	1206	12.29 ± 0.33	...	...
S II	1259	13.08 ± 0.10	-2.49 ± 0.11	$+0.45 \pm 0.11$
Fe II	1608, 2344, 2374, 2382, 2586, 2600	12.96 ± 0.05	-2.94 ± 0.06	...
Fe III	1122	$\leqslant 13.02$[a]	...	...

Note. [a] 3σ upper limit.

contributions of turbulent and thermal broadening; thermal broadening depends inversely on the square-root of the atom's mass, whereas turbulent broadening is the same for all gas constituents. Thus, one can measure the kinetic temperature of the absorbing gas cloud *directly*, provided that:

1. The gas in each absorption component is distributed according to a Maxwell–Boltzmann distribution;
2. An array of transitions of differing oscillator strengths from a given ion is available to populate the curve-of-growth and thereby measure the total broadening; and
3. Absorption lines from at least two atoms of widely differing mass are accessible to measure the thermal contribution to the line broadening. The ideal ions that satisfy these criteria are the light D I with its host of Lyman series transitions in combination with one of the heavier atoms (such as O I, Si II, or Fe II) which have a range of transitions with a variety of strengths and are commonly observed in DLAs. In some favorable cases (see Appendix B), it is also possible to solely use a selection of metal absorption lines to obtain a handle on the gas kinetic temperature (Carswell et al. 2012).

In many cases, the combined thermal and turbulent broadening of the metal line profiles is only marginally resolved from the instrumental broadening. An accurate measure of the instrumental profile is therefore required in order to pin down the cloud model of the absorbing gas. Moreover, if the point spread function of the quasar does not uniformly illuminate the spectrograph's slit, the instrumental resolution during the observations will be less than the nominal instrumental resolution measured from the widths of the ThAr arc lines. We overcome this uncertainty by assuming that the instrumental broadening function is closely approximated by a Gaussian, and allow the FWHM of the Gaussian profile to be a free parameter in our modeling procedure. Therefore, our uncertainty in the instrumental profile is folded into the uncertainty in both the cloud model and chemical abundances. Our profile analysis also folds in the uncertainty in the placement of the quasar continuum level, by fitting a low order polynomial to the quasar continuum during the absorption line fitting procedure.

DLAs are generally considered to host a CNM and a WNM in pressure equilibrium (e.g., Wolfire et al. 1995). We have performed a suite of Monte Carlo simulations to test the sensitivity of the above technique to the presence of a two-phase medium. We consider two test cases:

1. A system with only metal-absorption lines (J0035−0918), and
2. A system with metal, D I, and H I absorption lines (J1419+0829).

Using the best-fitting absorption line profiles, we generated a new model where 50 per cent of the gas along the line-of-sight resides in a CNM (100 K), and the remaining gas is in a WNM with the measured kinetic temperature. One hundred Monte Carlo realizations were generated by perturbing these model profiles by the error spectrum of the data. We first perform a fit to each realization that includes both a CNM *and* a WNM. On the basis of these simulations we conclude that we are unable to recover the properties of the CNM; our technique to measure the kinetic temperature is therefore insensitive to the presence of a CNM. We then performed a second fit to each realization but this time we only included a WNM component in the fit. With this test, we were able to recover the properties of the WNM, without any significant bias. Therefore, if the DLAs that we probe in our sample contain a CNM, the physical properties that we derive are largely unaffected, although we are unable to detect the presence of a CNM. In future studies, it may be possible to identify a CNM in metal-poor DLAs by detecting absorption from molecular hydrogen or C I. Absorption lines from these species are not present in our sample.

APPENDIX B
NEW SYSTEMS

The majority of our sample is described in our previous work (Pettini et al. 2008; Cooke et al. 2011b, 2014). In this Appendix, we present our analysis of a newly discovered metal-poor DLA at redshift $z_{abs} \simeq 2.271$ toward J1111+1332 and provide an improved reanalysis of the metal-poor DLA reported by Cooke et al. (2011a) at $z_{abs} \simeq 2.340$ toward J0035−0918. In both of these systems, the data cover absorption lines with a range of oscillator strengths for several elements between C and Ni. The difference in atomic mass for these elements, combined with the broad range of oscillator strengths for many transitions, has allowed us to decouple the thermal broadening of the line profile (which depends on the atomic mass) from that of turbulent broadening (assumed to be the same for all elements), using metal absorption lines alone.

B.1. J0035−0918, $z_{abs} = 2.340097$

The DLA at redshift $z_{abs} \simeq 2.340$ toward the quasar J0035−0918 is currently one of the most metal-poor systems known. It was initially reported by Cooke et al. (2011a) as

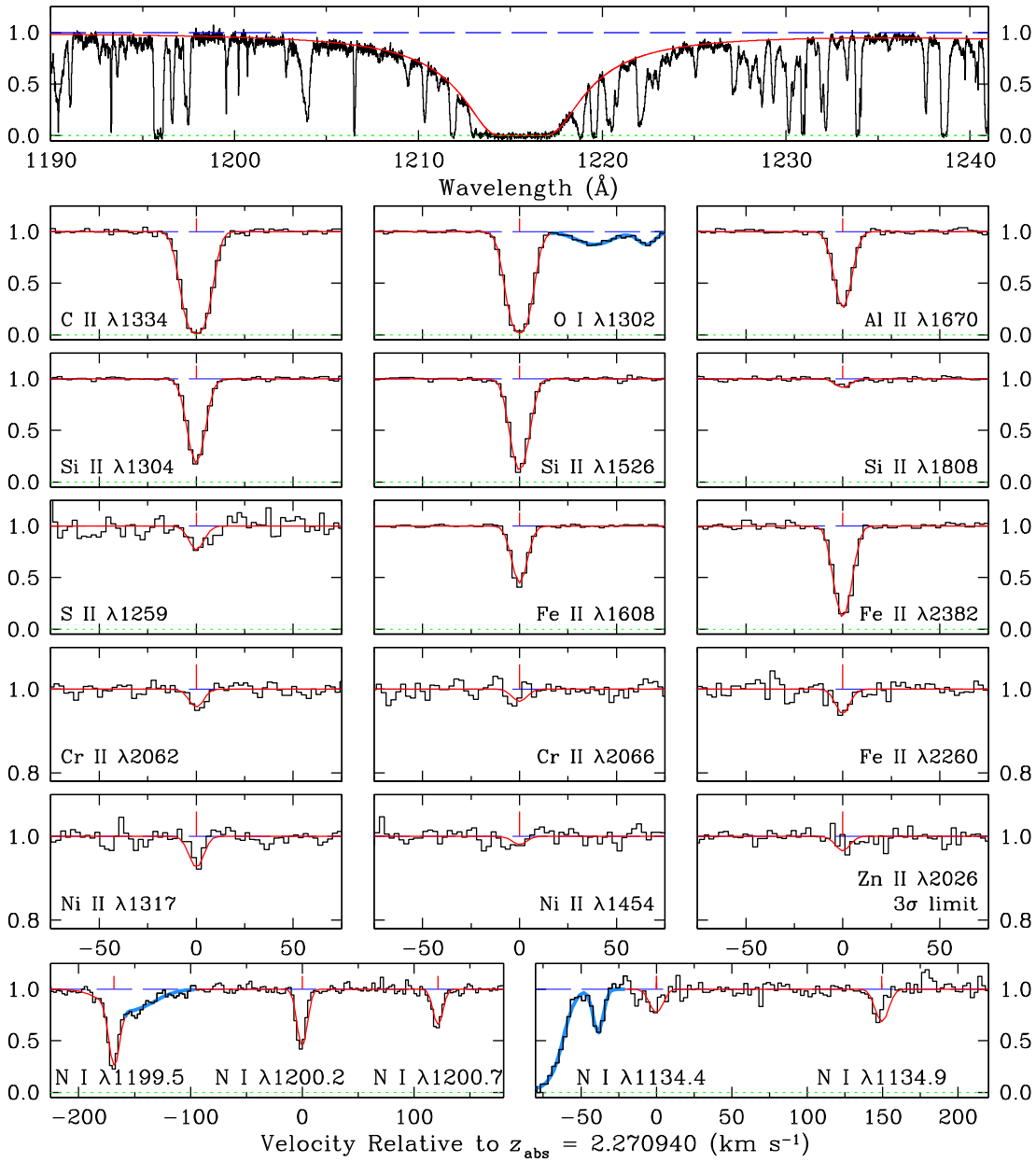

Figure 8. Top panel shows the damped Lyα line for the DLA at $z_{\rm abs} = 2.270940$ toward the QSO J1111+1332 (black histogram). The continuous red line is the best-fitting Voigt profile model for an H I column density $\log N({\rm H\,I})/{\rm cm}^{-2} = 20.39 \pm 0.04$. The remaining panels display a selection of the associated metal absorption lines, with the best-fitting model overplotted. Fitted line blends are shown by the blue lines. The red tick marks above the spectra indicate the position of the absorption component. Note the different y-axis scale used to expose the weak Cr II, Ni II, and Zn II lines, as well as Fe II λ2260. For Zn II λ2026, we overplot the cloud model for the derived 3σ upper limit. The normalized quasar continuum and zero-level are shown by the horizontal blue long-dashed and green dotted lines, respectively. The red wing of the Lyα profile is slightly depressed relative to the QSO continuum due to another DLA along this sightline at $z_{\rm abs} \simeq 2.38223$.

the first known example of a DLA with an abundance pattern resembling the nucleosynthesis expected by the first stars. In particular, this DLA was reported to have an abnormal excess of C and N relative to Fe, [C/Fe]=+1.53. This result was later contested by Carswell et al. (2012), who correctly pointed out that a contribution from thermal broadening would result in a lower overabundance of C/Fe. Using the Cooke et al. (2011a) data, these authors estimated the carbon overabundance for this system to be [C/Fe] +0.51 ± 0.10 for a cloud model that is purely broadened by thermal motions; this value is a theoretical lower limit on the true [C/Fe] abundance for this system, which is likely broadened by both mechanisms. Unfortunately, the initial data reported by Cooke et al. (2011a) did not cover several important N I and Fe II absorption lines with a high oscillator strength which would have permitted a decoupling of the thermal and turbulent motions.

By combining the Cooke et al. (2011a) data with the recent observations described by Dutta et al. (2014), we find that a single component at redshift $z_{\rm abs} = 2.340097 \pm 0.000001$ provides an excellent fit to the data, with a turbulent Doppler parameter $b_{\rm turb} = 1.1 \pm 0.4$ and a temperature $T_{\rm gas} = 7800 \pm 1600$. Using the new, high-resolution UVES spectrum, we derive an H I column density from the Lyα transition $\log N({\rm H\,I})/{\rm cm}^{-2} = 20.43 \pm 0.04$. This estimate is lower by ∼0.1 dex from that reported by Cooke et al. (2011a), who used a medium resolution spectrum from the Magellan Echellette spectrograph to derive N(H I). The overabundance of C relative to Fe for our best-fit model is [C/Fe] = +0.58 ± 0.16, implying that thermal

Table 6
Ion Column Densities of the DLA in J1111 + 1332 at $z_{abs} = 2.270940$

Ion	Transitions Used	log N(X)/cm^{-2}	[X/H]	[X/Fe]
H I	1215	20.39 ± 0.04	...	...
C II	1334	14.72 ± 0.09	-2.10 ± 0.10	$+0.17 \pm 0.09$
N I	1134.4, 1134.9, 1199.5, 1200.2, 1200.7	13.53 ± 0.02	-2.69 ± 0.05	-0.42 ± 0.02
O I	1302	15.16 ± 0.07	-1.92 ± 0.08	$+0.35 \pm 0.07$
Al II	1670	12.37 ± 0.02	-2.46 ± 0.05	-0.19 ± 0.02
Al III	1854, 1862	11.90 ± 0.03	...	...
Si II	1190, 1193, 1260, 1304, 1526, 1808	13.95 ± 0.02	-1.95 ± 0.05	$+0.32 \pm 0.02$
Si III	1206	13.36 ± 0.05	...	...
Si IV	1393, 1402	13.09 ± 0.02	...	...
S II	1259	13.69 ± 0.09	-1.84 ± 0.10	$+0.43 \pm 0.09$
Cr II	2062, 2066	12.00 ± 0.09	-2.03 ± 0.10	$+0.24 \pm 0.09$
Fe II	1121, 1125, 1143, 1144, 1608, 1611, 2260, 2374, 2382	13.59 ± 0.01	-2.27 ± 0.04	...
Ni II	1317, 1370, 1454, 1751	12.15 ± 0.06	-2.45 ± 0.07	-0.18 ± 0.06
Zn II	2026	$\leqslant 11.08$[a]	$\leqslant -1.94$	$\leqslant +0.33$

Note. [a] 3σ upper limit.

broadening does indeed contribute significantly to the cloud kinematics of this DLA. For compariosn, Dutta et al. (2014) deduced [C/Fe] = $+0.45 \pm 0.19$, which is consistent with, but somewhat lower than, the minimum value estimated by Carswell et al. (2012) for a purely thermally broadened cloud model. Nevertheless, our analysis is consistent with their estimate. The derived column densities for this system are collected in Table 5. Overall, this DLA still exhibits an enhancement in C/Fe, greater than that exhibited by a typical very metal-poor DLA by 2.4σ; however, it no longer meets the generally adopted criterion defining carbon-enhanced metal-poor (CEMP) stars, [C/Fe] $\geqslant$ +0.7 (Aoki et al. 2007). Although this system is not quite as abundant in carbon as once thought, it is certainly a chemically peculiar system and highlights the need to push these studies to even lower metallicities where such anomalous abundance patterns are expected to be more common (Cooke & Madau 2014).

B.2. J1111+1332, $z_{abs} = 2.270940$

The second system reported here is the $z_{abs} \simeq 2.271$ DLA toward the $m_r \simeq 17.1$ quasar J1111 + 1332. We first recognized this DLA as an excellent candidate VMP DLA from the relatively high S/N SDSS discovery spectrum, which exhibits strong H I Lyα absorption line together with the apparent absence of associated metal absorption lines. We performed follow-up observations of J1111 + 1332 with HIRES (Vogt et al. 1994) on 2011 March 24 and 25 (Program ID: A152Hb). We employed the 1.148 arcsec wide C5 decker (with a nominal resolution of $v_{FWHM} = 8.3$ km s^{-1}) and the red cross-disperser. We recorded 6×2700 s exposures, covering a wavelength range 4645–8155 with small gaps near 5100 Å and 6700 Å. We used 2×2 on-chip binning. The data were reduced with MAKEE,[14] following the standard reduction steps of bias subtraction and flat fielding. The orders were defined and traced using a quartz lamp exposure with a pinhole decker (D5). After the orders were extracted, the data were converted to a vacuum heliocentric wavelength frame, with reference to an exposure of a ThAr hollow-cathode lamp. The final spectrum was combined with UVES_POPLER.[15] The combined S/N of the data near 6000 Å is ~60.

Cooke et al. (2013) included the Fe-peak element ratios in this DLA in their study. Here, we report a detailed profile analysis which includes all of the available metal species. In total, we detect the absorption lines for 10 elements and place an interesting upper limit on the Zn abundance. The absorption profiles are very well fit by a single absorption component centered at redshift $z_{abs} = 2.270940 \pm 0.000001$ with turbulent Doppler parameter $b_{turb} = 2.2 \pm 0.1$ km s^{-1} and gas kinetic temperature $T_{gas} = 13{,}000 \pm 2000$ K. We reproduce the data and our best-fitting model for this system in Figure 8 where the top panel shows the damped Lyα line profile, and best-fitting model for log N(H I)/cm^{-2} = 20.39 ± 0.04. The remaining panels are a selection of metal absorption lines. The y-axis scale has been reduced in the six panels showing the weakest absorption lines. Column densities for all detected elements and ion stages in this system are collected in Table 6.

[14] MAKEE is maintained by T. Barlow and is available from http://www.astro.caltech.edu/~tb/makee/.
[15] UVES_POPLER was written and is maintained by M. T. Murphy, and is available from http://astronomy.swin.edu.au/~mmurphy/UVES_popler/.

REFERENCES

Akerman, C. J., Ellison, S. L., Pettini, M., & Steidel, C. C. 2005, A&A, 440, 499
Alavi, A., Siana, B., Richard, J., et al. 2014, ApJ, 780, 143
Amorín, R., Grazian, A., Castellano, M., et al. 2014, ApJL, 788, L4
Aoki, W., Beers, T. C., Christlieb, N., et al. 2007, ApJ, 655, 492
Asplund, M., Grevesse, N., Sauval, A. J., & Scott, P. 2009, ARA&A, 47, 481
Barnes, L. A., & Haehnelt, M. G. 2014, MNRAS, 440, 2313
Belokurov, V. 2013, NewAR, 57, 100
Belokurov, V., Zucker, D. B., Evans, N. W., et al. 2006, ApJL, 647, L111
Bensby, T., Feltzing, S., Lundström, I., & Ilyin, I. 2005, A&A, 433, 185
Bernstein-Cooper, E. Z., Cannon, J. M., Elson, E. C., et al. 2014, AJ, 148, 35
Bird, S., Haehnelt, M., Neeleman, M., et al. 2014, arXiv:1407.7858
Bird, S., Vogelsberger, M., Sijacki, D., et al. 2013, MNRAS, 429, 3341
Bonifacio, P., Hill, V., Molaro, P., et al. 2000, A&A, 359, 663
Bonifacio, P., Sbordone, L., Marconi, G., Pasquini, L., & Hill, V. 2004, A&A, 414, 503
Bromm, V., & Yoshida, N. 2011, ARA&A, 49, 373
Bullock, J. S., Kravtsov, A. V., & Weinberg, D. H. 2000, ApJ, 539, 517
Bunker, A. J., Warren, S. J., Clements, D. L., Williger, G. M., & Hewett, P. C. 1999, MNRAS, 309, 875
Cantalupo, S., Lilly, S. J., & Haehnelt, M. G. 2012, MNRAS, 425, 1992
Carswell, R. F., Becker, G. D., Jorgenson, R. A., Murphy, M. T., & Wolfe, A. M. 2012, MNRAS, 422, 1700
Cen, R. 2012, ApJ, 748, 121
Chieffi, A., & Limongi, M. 2004, ApJ, 608, 405
Christensen, L., Møller, P., Fynbo, J. P. U., & Zafar, T. 2014, MNRAS, 445, 225
Christensen, L., Noterdaeme, P., Petitjean, P., Ledoux, C., & Fynbo, J. P. U. 2009, A&A, 505, 1007
Cohen, J. G., & Huang, W. 2009, ApJ, 701, 1053
Cohen, J. G., & Huang, W. 2010, ApJ, 719, 931

Cooke, J., Wolfe, A. M., Gawiser, E., & Prochaska, J. X. 2006, ApJ, 652, 994
Cooke, R., & Madau, P. 2014, ApJ, 791, 116
Cooke, R., Pettini, M., Jorgenson, R. A., et al. 2013, MNRAS, 431, 1625
Cooke, R. J., Pettini, M., Jorgenson, R. A., Murphy, M. T., & Steidel, C. C. 2014, ApJ, 781, 31
Cooke, R., Pettini, M., & Murphy, M. T. 2012, MNRAS, 425, 347
Cooke, R., Pettini, M., Steidel, C. C., Rudie, G. C., & Jorgenson, R. A. 2011a, MNRAS, 412, 1047
Cooke, R., Pettini, M., Steidel, C. C., Rudie, G. C., & Nissen, P. E. 2011b, MNRAS, 417, 1534
de Boer, T. J. L., Belokurov, V., Beers, T. C., & Lee, Y. S. 2014, MNRAS, 443, 658
Dutta, R., Srianand, R., Rahmani, H., et al. 2014, MNRAS, 440, 307
Ellison, S. L., Prochaska, J. X., Hennawi, J., et al. 2010, MNRAS, 406, 1435
Ferland, G. J., Porter, R. L., van Hoof, P. A. M., et al. 2013, RMxAA, 49, 137
Font-Ribera, A., Miralda-Escud, J., Arnau, E., et al. 2012, JCAP, 11, 059
Frebel, A., & Bromm, V. 2012, ApJ, 759, 115
Frebel, A., Simon, J. D., & Kirby, E. N. 2014, ApJ, 786, 74
Fumagalli, M., O'Meara, J. M., Prochaska, J. X., Kanekar, N., & Wolfe, A. M. 2014, MNRAS, 444, 1282
Fumagalli, M., Prochaska, J. X., Kasen, D., et al. 2011, MNRAS, 418, 1796
Fynbo, J. P. U., Laursen, P., Ledoux, C., et al. 2010, MNRAS, 408, 2128
Gilmore, G., Norris, J. E., Monaco, L., et al. 2013, ApJ, 763, 61
Giovanelli, R., Haynes, M. P., Adams, E. A. K., et al. 2013, AJ, 146, 15
Haardt, F., & Madau, P. 2012, ApJ, 746, 125
Haehnelt, M. G., Steinmetz, M., & Rauch, M. 1998, ApJ, 495, 647
Heger, A., & Woosley, S. E. 2010, ApJ, 724, 341
Heiles, C., & Troland, T. H. 2003, ApJ, 586, 1067
Hendricks, B., Koch, A., Lanfranchi, G. A., et al. 2014, ApJ, 785, 102
Hill, V., Barbuy, B., & Spite, M. 1997, A&A, 323, 461
Hill, V., & DART Collaboration, 2012, in ASP Conf. Ser. 458, Galactic Archaeology: Near-Field Cosmology and the Formation of the Milky Way, ed. W. Aoki, M. Ishigaki, T. Suda, T. Tsujimoto, & N. Arimoto (San Francisco, CA: ASP), 297
Howk, J. C., Wolfe, A. M., & Prochaska, J. X. 2005, ApJ, 622, L81
Illingworth, G. D., Magee, D., Oesch, P. A., et al. 2013, ApJS, 209, 6
Jenkins, E. B., & Tripp, T. M. 2001, ApJS, 137, 297
Jenkins, E. B., & Tripp, T. M. 2006, ApJ, 637, 548
Jenkins, E. B., & Tripp, T. M. 2011, ApJ, 734, 65
Jorgenson, R. A., Murphy, M. T., & Thompson, R. 2013, MNRAS, 435, 482
Jorgenson, R. A., Murphy, M. T., Thompson, R., & Carswell, R. F. 2014, MNRAS, 443, 2783
Jorgenson, R. A., & Wolfe, A. M. 2014, ApJ, 785, 16
Jorgenson, R. A., Wolfe, A. M., & Prochaska, J. X. 2010, ApJ, 722, 460
Jorgenson, R. A., Wolfe, A. M., Prochaska, J. X., & Carswell, R. F. 2009, ApJ, 704, 247
Kanekar, N., & Chengalur, J. N. 2001, A&A, 369, 42
Kanekar, N., Prochaska, J. X., Smette, A., et al. 2014, MNRAS, 438, 2131
Kirby, E. N., Cohen, J. G., Smith, G. H., et al. 2011a, ApJ, 727, 79
Kirby, E. N., Lanfranchi, G. A., Simon, J. D., Cohen, J. G., & Guhathakurta, P. 2011b, ApJ, 727, 78
Koch, A., Grebel, E. K., Gilmore, G. F., et al. 2008, AJ, 135, 1580
Kowal, G., Lazarian, A., & Beresnyak, A. 2007, ApJ, 658, 423
Krogager, J.-K., Fynbo, J. P. U., Ledoux, C., et al. 2013, MNRAS, 433, 3091
Krogager, J.-K., Fynbo, J. P. U., Møller, P., et al. 2012, MNRAS, 424, L1
Kulkarni, V. P., Hill, J. M., Schneider, G., et al. 2000, ApJ, 536, 36
Lai, D. K., Lee, Y. S., Bolte, M., et al. 2011, ApJ, 738, 51
Ledoux, C., Petitjean, P., Fynbo, J. P. U., Møller, P., & Srianand, R. 2006, A&A, 457, 71
Letarte, B., Hill, V., Tolstoy, E., et al. 2010, A&A, 523, A17
Liszt, H. 2001, A&A, 371, 698
Lowenthal, J. D., Hogan, C. J., Green, R. F., et al. 1995, ApJ, 451, 484
Mannucci, F., Della Valle, M., & Panagia, N. 2006, MNRAS, 370, 773
Maio, U., Tescari, E., & Cooke, R. 2014, MNRAS, submitted
Markwardt, C. B. 2009, in ASP Conf. Ser. 411, Astronomical Data Analysis Software and Systems XVIII, ed. D. A. Bohlender, D. Durand, & P. Dowler (San Francisco, CA: ASP), 251
Mateo, M. L. 1998, ARA&A, 36, 435
McConnachie, A. W. 2012, AJ, 144, 4
McKee, C. F., & Ostriker, E. C. 2007, ARA&A, 45, 565
Møller, P., Fynbo, J. P. U., Ledoux, C., & Nilsson, K. K. 2013, MNRAS, 430, 2680
Monaco, L., Bellazzini, M., Bonifacio, P., et al. 2005, A&A, 441, 141
Morton, D. C. 2003, ApJS, 149, 205
Morton, D. C., Drake, J. F., Jenkins, E. B., et al. 1973, ApJL, 181, L103
Murphy, M. T., & Berengut, J. C. 2014, MNRAS, 438, 388
Murphy, M. T., Curran, S. J., Webb, J. K., Ménager, H., & Zych, B. J. 2007, MNRAS, 376, 673
Neeleman, M., Wolfe, A. M., Prochaska, J. X., & Rafelski, M. 2013, ApJ, 769, 54
Norris, J. E., Wyse, R. F. G., Gilmore, G., et al. 2010, ApJ, 723, 1632
Noterdaeme, P., Laursen, P., Petitjean, P., et al. 2012, A&A, 540, A63
Penprase, B. E., Prochaska, J. X., Sargent, W. L. W., Toro-Martinez, I., & Beeler, D. J. 2010, ApJ, 721, 1
Péroux, C., Bouché, N., Kulkarni, V. P., York, D. G., & Vladilo, G. 2012, MNRAS, 419, 3060
Petitjean, P., Srianand, R., & Ledoux, C. 2000, A&A, 364, L26
Pettini, M., & Cooke, R. 2012, MNRAS, 425, 2477
Pettini, M., Hunstead, R. W., Murdoch, H. S., & Blades, J. C. 1983, ApJ, 273, 436
Pettini, M., King, D. L., Smith, L. J., & Hunstead, R. W. 1997, ApJ, 478, 536
Pettini, M., Zych, B. J., Steidel, C. C., & Chaffee, F. H. 2008, MNRAS, 385, 2011
Pompéia, L., Hill, V., Spite, M., et al. 2008, A&A, 480, 379
Pontzen, A., Governato, F., Pettini, M., et al. 2008, MNRAS, 390, 1349
Prochaska, J. X., Chen, H.-W., Wolfe, A. M., Dessauges-Zavadsky, M., & Bloom, J. S. 2008, ApJ, 672, 59
Prochaska, J. X., Gawiser, E., Wolfe, A. M., Cooke, J., & Gelino, D. 2003, ApJS, 147, 227
Prochaska, J. X., & Wolfe, A. M. 1997, ApJ, 487, 73
Prochaska, J. X., & Wolfe, A. M. 2010, arXiv:1009.3960
Rafelski, M., Wolfe, A. M., Prochaska, J. X., Neeleman, M., & Mendez, A. J. 2012, ApJ, 755, 89
Rahmati, A., & Schaye, J. 2014, MNRAS, 438, 529
Rauch, M., Haehnelt, M., Bunker, A., et al. 2008, ApJ, 681, 856
Redfield, S., & Linsky, J. L. 2004, ApJ, 613, 1004
Ryan, S. G., Aoki, W., Norris, J. E., & Beers, T. C. 2005, ApJ, 635, 349
Ryan-Weber, E. V., Begum, A., Oosterloo, T., et al. 2008, MNRAS, 384, 535
Saito, Y.-J., Takada-Hidai, M., Honda, S., & Takeda, Y. 2009, PASJ, 61, 549
Salvadori, S., & Ferrara, A. 2012, MNRAS, 421, L29
Sbordone, L., Bonifacio, P., Buonanno, R., et al. 2007, A&A, 465, 815
Shetrone, M. D., Bolte, M., & Stetson, P. B. 1998, AJ, 115, 1888
Shetrone, M. D., Côté, P., & Sargent, W. L. W. 2001, ApJ, 548, 592
Skillman, E. D., Salzer, J. J., Berg, D. A., et al. 2013, AJ, 146, 3
Srianand, R., Gupta, N., Petitjean, P., et al. 2012, MNRAS, 421, 651
Srianand, R., Petitjean, P., Ledoux, C., Ferland, G., & Shaw, G. 2005, MNRAS, 362, 549
Starkenburg, E., Hill, V., Tolstoy, E., et al. 2013, A&A, 549, A88
Tescari, E., Viel, M., Tornatore, L., & Borgani, S. 2009, MNRAS, 397, 411
Tinsley, B. M. 1979, ApJ, 229, 1046
Tolstoy, E., Hill, V., & Tosi, M. 2009, ARA&A, 47, 371
Tolstoy, E., & Saha, A. 1996, ApJ, 462, 672
Tumlinson, J., Malec, A. L., Carswell, R. F., et al. 2010, ApJL, 718, L156
Vallerga, J. 1996, SSRv, 78, 277
van de Voort, F., Schaye, J., Altay, G., & Theuns, T. 2012, MNRAS, 421, 2809
Vargas, L. C., Geha, M. C., & Tollerud, E. J. 2014, ApJ, 790, 73
Venn, K. A. 1999, ApJ, 518, 405
Venn, K. A., Irwin, M., Shetrone, M. D., et al. 2004, AJ, 128, 1177
Vladilo, G., Abate, C., Yin, J., Cescutti, G., & Matteucci, F. 2011, A&A, 530, A33
Vogt, S. S., Allen, S. L., Bigelow, B. C., et al. 1994, Proc. SPIE, 2198, 362
Walker, M. 2013, in Planets, Stars and Stellar Systems. Vol. 5: Galactic Structure and Stellar Populations (Dordrecht: Springer), 1039
Weisz, D. R., Dalcanton, J. J., Williams, B. F., et al. 2011, ApJ, 739, 5
Weisz, D. R., Dolphin, A. E., Skillman, E. D., et al. 2014a, ApJ, 789, 147
Weisz, D. R., Dolphin, A. E., Skillman, E. D., et al. 2014b, ApJ, 789, 148
Wheeler, J. C., Sneden, C., & Truran, J. W., Jr. 1989, ARA&A, 27, 279
Willman, B., Blanton, M. R., West, A. A., et al. 2005a, AJ, 129, 2692
Willman, B., Dalcanton, J. J., Martinez-Delgado, D., et al. 2005b, ApJL, 626, L85
Wolfe, A. M., Gawiser, E., & Prochaska, J. X. 2005, ARA&A, 43, 861
Wolfe, A. M., Prochaska, J. X., & Gawiser, E. 2003, ApJ, 593, 215
Wolfe, A. M., Turnshek, D. A., Smith, H. E., & Cohen, R. D. 1986, ApJS, 61, 249
Wolfire, M. G., Hollenbach, D., McKee, C. F., Tielens, A. G. G. M., & Bakes, E. L. O. 1995, ApJ, 443, 152
Wolfire, M. G., McKee, C. F., Hollenbach, D., & Tielens, A. G. G. M. 2003, ApJ, 587, 278
Woosley, S. E., & Weaver, T. A. 1995, ApJS, 101, 181
York, D. G., Adelman, J., Anderson, J. E., Jr., et al. 2000, AJ, 120, 1579